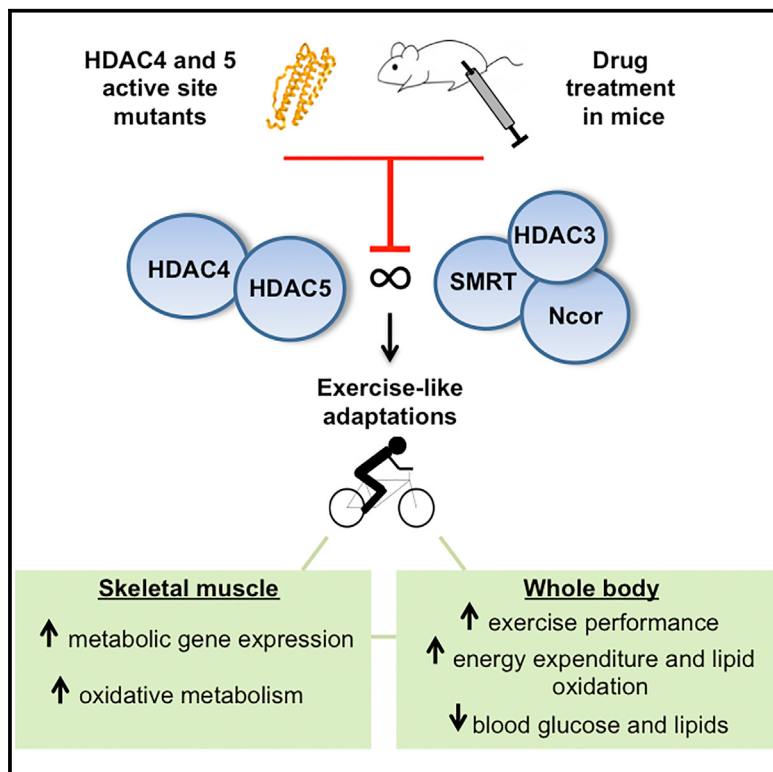


Disruption of the Class IIa HDAC Corepressor Complex Increases Energy Expenditure and Lipid Oxidation

Graphical Abstract



Authors

Vidhi Gaur, Timothy Connor,
Andrew Sanigorski, ..., Ken R. Walder,
Mark Hargreaves, Sean L. McGee

Correspondence

sean.mcgee@deakin.edu.au

In Brief

Physical inactivity is a major cause of chronic diseases. Drugs that mimic aspects of exercise could therefore reduce chronic disease burden. Gaur et al. identify and validate the class IIa histone deacetylases (HDACs) as drug targets to replicate aspects of the exercise adaptive response.

Highlights

- HDAC4/5 active-site mutants increase exercise-responsive genes and metabolism
- Scriptaid is a compound with similar phenotypic effects *in vitro*
- Acute Scriptaid administration in mice increases exercise-responsive genes
- Chronic Scriptaid administration reduces blood glucose and lipids in mice

Accession Numbers

GSE54642

Disruption of the Class IIa HDAC Corepressor Complex Increases Energy Expenditure and Lipid Oxidation

Vidhi Gaur,^{1,11} Timothy Connor,^{1,11} Andrew Sanigorski,¹ Sheree D. Martin,¹ Clinton R. Bruce,² Darren C. Henstridge,³ Simon T. Bond,¹ Kevin A. McEwen,¹ Lyndal Kerr-Bayles,¹ Trent D. Ashton,⁴ Cassandra Fleming,⁴ Min Wu,⁵ Lisa S. Pike Winer,⁵ Denise Chen,⁵ Gregg M. Hudson,⁶ John W.R. Schwabe,⁶ Keith Baar,⁷ Mark A. Febbraio,^{3,8} Paul Gregorevic,⁹ Frederick M. Pfeffer,⁴ Ken R. Walder,¹ Mark Hargreaves,¹⁰ and Sean L. McGee^{1,3,12,*}

¹Metabolic Research Unit, School of Medicine, Deakin University, Waurn Ponds, VIC 3216, Australia

²School of Exercise and Nutrition Sciences, Deakin University, Burwood, VIC 3125, Australia

³Metabolism and Inflammation Program, Baker IDI Heart and Diabetes Institute, Melbourne, VIC 3004, Australia

⁴Research Centre for Chemistry and Biotechnology, School of Life and Environmental Sciences, Deakin University, Waurn Ponds, VIC 3216, Australia

⁵Seahorse Bioscience, North Billerica, MA 01862, USA

⁶Department of Biochemistry, Henry Wellcome Laboratories of Structural Biology, University of Leicester, Leicester LE1 7RH, UK

⁷Department of Neurobiology, Physiology and Behavior and Department of Physiology and Membrane Biology, University of California, Davis, Davis, CA 95616, USA

⁸Division of Diabetes & Metabolism, Garvan Institute of Medical Research, Darlinghurst, Sydney, NSW 2010, Australia

⁹Muscle Research and Therapeutics Laboratory, Baker IDI Heart and Diabetes Institute, Melbourne, VIC 3004, Australia

¹⁰Department of Physiology, The University of Melbourne, Parkville, VIC 3010, Australia

¹¹Co-first author

¹²Lead Contact

*Correspondence: sean.mcgee@deakin.edu.au

<http://dx.doi.org/10.1016/j.celrep.2016.08.005>

SUMMARY

Drugs that recapitulate aspects of the exercise adaptive response have the potential to provide better treatment for diseases associated with physical inactivity. We previously observed reduced skeletal muscle class IIa HDAC (histone deacetylase) transcriptional repressive activity during exercise. Here, we find that exercise-like adaptations are induced by skeletal muscle expression of class IIa HDAC mutants that cannot form a corepressor complex. Adaptations include increased metabolic gene expression, mitochondrial capacity, and lipid oxidation. An existing HDAC inhibitor, Scriptaid, had similar phenotypic effects through disruption of the class IIa HDAC corepressor complex. Acute Scriptaid administration to mice increased the expression of metabolic genes, which required an intact class IIa HDAC corepressor complex. Chronic Scriptaid administration increased exercise capacity, whole-body energy expenditure and lipid oxidation, and reduced fasting blood lipids and glucose. Therefore, compounds that disrupt class IIa HDAC function could be used to enhance metabolic health in chronic diseases driven by physical inactivity.

INTRODUCTION

Physical inactivity, which is related to energy imbalance and a loss of functional capacity (Booth et al., 2012), is recognized as a major cause of chronic disease and mortality (Mokdad et al., 2004). However, many patients and at-risk individuals do not, or cannot, engage in physical activity. Identification of the mechanisms mediating exercise adaptations could provide new molecular targets for therapeutic intervention.

Adaptations to exercise involve repeated transient changes in gene expression that alter protein levels and, ultimately, phenotype (Egan and Zierath, 2013). A number of studies implicate the class IIa histone deacetylase (HDAC) myocyte enhancer factor 2 (MEF2) axis in this process. The class IIa HDACs, which include isoforms 4, 5, 7, and 9, repress gene expression by interacting with the MEF2 transcription factors (McKinsey et al., 2001). Although the catalytic domain of the class IIa HDACs is structurally similar to the highly active class I HDACs, they have low intrinsic HDAC activity against acetyl-lysine substrates due to a single amino acid substitution within their active site (Lahm et al., 2007), and their repressive activity requires a corepressor complex that contains SMRT/N-Cor and HDAC3 (Fischle et al., 2002; Kao et al., 2000), a class I HDAC. We have found that this class IIa HDAC corepressor complex is disrupted by exercise in human skeletal muscle through phosphorylation-dependent nuclear export of HDAC4 and HDAC5 (McGee et al., 2009), which reduced their association with MEF2 (McGee and Hargreaves, 2004), increased MEF2 DNA binding (McGee

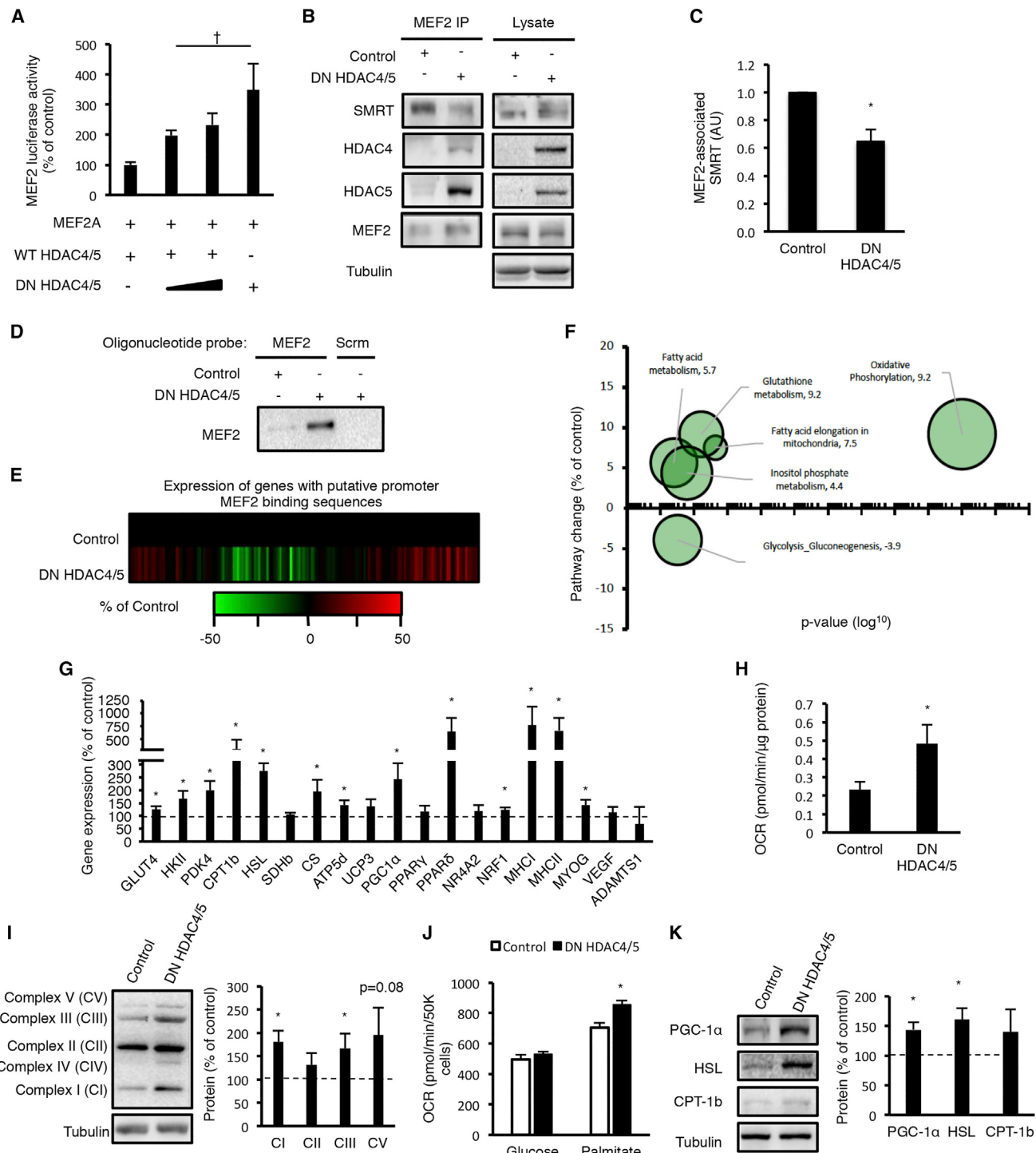


Figure 1. Active-Site Mutants DN HDAC4 and 5 Increase MEF2 Transcriptional Activity, the Expression of Exercise-Responsive Genes, and Oxidative Metabolism

(A) MEF2 luciferase reporter assays with various combinations of MEF2A, HDAC4, and HDAC5, with increasing amounts of DN HDAC4 and 5 (n = 3 biological replicates per group).

(B) Coimmunoprecipitation of the class IIa HDAC corepressor complex from extensor digitorum longus (EDL) muscles administered with empty rAAV6 (Control) or rAAV6 DN HDAC4 and rAAV6 DN HDAC5 via intramuscular injection.

(legend continued on next page)

et al., 2006), and increased expression of MEF2-dependent genes (McGee and Hargreaves, 2004). However, the role of MEF2 in muscle post-development is unclear. Similarly, the gene networks that the class Ila HDACs regulate in adult muscle are unknown. Further understanding of this signaling axis could reveal the class Ila HDACs as targets for pharmacological induction of exercise adaptions.

Most HDAC inhibitors lack isoform selectivity and generally consist of a chelating moiety that interacts with the active-site zinc atom, a narrow linker region that spans the catalytic groove and a capping group (Sternson et al., 2001). It has emerged that some HDAC inhibitors can disrupt the class Ila HDAC corepressor complex by changing the conformation of the class Ila HDAC active site, which mediates physical association with N-Cor/SMRT (Hudson et al., 2015; Lahm et al., 2007). Therefore, HDAC inhibitors that were thought to only inhibit class I HDAC catalytic activity may have efficacy against class Ila HDAC transcriptional repression. Here, we found that expression of class Ila HDAC active-site mutants that disrupt their corepressor complex in skeletal muscle induced metabolic adaptations and identified a HDAC inhibitor, Scriptaid, which had similar phenotypic effects. Moreover, chronic administration of Scriptaid to mice induced skeletal muscle and systemic metabolic adaptive responses.

RESULTS

Active-Site Mutant HDAC4 and HDAC5 Increase MEF2 Transcriptional Activity, the Expression of Metabolic Genes, and Oxidative Metabolism

Mutation of key residues within the active site of class Ila HDACs disrupts the class Ila HDAC corepressor complex in vitro (Fischle et al., 2002; Hudson et al., 2015); however, the effect on MEF2 activity is unknown. In a MEF2 reporter assay that was sensitive to HDAC repression (Figures S1A and S1B), expression of HDAC4 and HDAC5 active-site mutants (D840N HDAC4 and D870N HDAC5 in human; D832N HDAC4 and D861N HDAC5 in mouse) increased MEF2-dependent transcription (Figure 1A), which required mutation of both HDAC4 and HDAC5 (data not shown). This shows that the D832N HDAC4 and D861N HDAC5 mutants (referred to hereinafter as DN HDAC4 and 5) act in a dominant-negative manner on MEF2-dependent transcription. To determine whether these mutants dissociated the class Ila corepressor complex in vivo, rAAV6 vectors expressing DN HDAC4 and 5 were administered to one hindlimb of C57BL6 mice via multiple intramuscular injections. The contralateral hindlimb musculature was administered with empty rAAV6 vector

as a control (Figure 1B). Class Ila HDAC transcriptional repression is mediated, in part, through their association with SMRT (Hudson et al., 2015). Coimmunoprecipitation showed that MEF2-associated SMRT was reduced in extensor digitorum longus (EDL) muscles expressing DN HDAC4 and 5 (Figures 1B and 1C). To examine the capacity for MEF2 to bind DNA, a biotinylated oligonucleotide pull-down assay with probes containing either a MEF2 consensus binding sequence or a scrambled sequence was validated (Figure S1C). Oligonucleotide binding by MEF2 was increased by DN HDAC4 and 5 expression (Figure 1D). To determine the transcriptional response to DN HDAC4 and 5 expression, microarray analyses were performed. The expression of ~60% of genes with a putative MEF2 binding sequence (CTAAAAATAG) in their promoter region was increased (Figure 1E), and 1,412 genes, primarily involved in metabolic processes (Figure S1D), were differentially expressed by DN HDAC4 and 5 expression. Gene set enrichment analysis (GSEA) of metabolic pathways using the entire microarray dataset revealed that oxidative phosphorylation, fatty acid metabolism, glutathione metabolism, inositol phosphate metabolism, and fatty acid elongation pathways were significantly increased by DN HDAC4 and 5 expression (Figure 1F). This was further examined by qRT-PCR. Exercise-responsive genes involved in glucose (*HKII* and *GLUT4*), lipid (*PDK4*, *CPT-1b*, and *HSL*), mitochondrial (*CS* and *ATP5b*), and transcriptional (*PGC-1 α* and *PPAR δ*) regulation of metabolism were increased by DN HDAC4 and 5 expression, in addition to genes involved in muscle fiber type determination (*MHC I* and *II*, *MYOG*; Figure 1G). To test whether oxidative capacity was enhanced, respiration was assessed in the tibialis anterior (TA) muscle of mice administered rAAV6 vectors expressing DN HDAC4 and 5 or control rAAV6. State 3 respiration was higher in muscles expressing DN HDAC4 and 5 (Figure 1H), and components of mitochondrial oxidative phosphorylation complexes were increased (Figure 1I; complex IV subunits could not be reliably detected in these samples and were not quantified). To dissect oxidative metabolism further, DN HDAC4 and 5 were expressed in C2C12 myotubes (Figure S1F), which increased basal oxygen consumption rate (OCR; Figure S1F). Analysis of mitochondrial function revealed that this was due to an increase in ATP turnover and not due to alterations in uncoupled respiration (Figure S1G), indicating an increase in cell-autonomous energy expenditure through processes that consume ATP. Analysis of basal glucose and lipid oxidation showed that DN HDAC4 and 5 expression increased oxidation of the fatty acid palmitate but not glucose (Figure 1J). The expression of DN HDAC4 and 5 in the EDL also increased the protein levels of PGC-1 α and HSL (Figure 1K), key regulatory

(C–F) MEF2-associated SMRT (C); MEF2 binding to an oligonucleotide probe with a consensus MEF2 binding site or a Scrambled (Scrm) sequence (D); Expression of genes with putative MEF2 promoter sequences (E); and bubble-plot representation of GSEA of metabolic pathways significantly altered by DN HDAC4 and 5 expression relative to control (empty rAAV6) in EDL muscle (F) (n = 5 per group).

(G–I) Expression profiles of exercise-responsive genes (G); oxygen consumption rate (OCR) measured under state 3 respiration conditions in tibialis anterior (TA) muscle (H); and (I) oxidative phosphorylation complex subunit protein in EDL muscle in mice administered empty rAAV6 (Control) or rAAV6 DN HDAC4 and rAAV6 DN HDAC5 (n = 10 per group).

(J) Substrate oxidation in C2C12 myotubes administered empty rAAV6 (Control) or rAAV6 DN HDAC4 and rAAV6 DN HDAC5 (n = 5 biological replicates per group).

(K) PGC-1 α , HSL, and CPT-1b protein following DN HDAC4 and HDAC5 expression relative to control in EDL muscle (n = 6 per group).

Data are means \pm SEM. † Versus cells expressing MEF2A and wild-type (WT) HDAC4 and HDAC5. *Versus control group. #Significantly enriched in dataset.

proteins involved in skeletal muscle lipid metabolism. Together, these data show that expression of class IIa HDAC active-site mutants that disrupt their corepressor complex enhanced the expression of metabolic genes and increased cell-autonomous energy expenditure that was supported by the oxidation of fatty acids.

Scriptaid Increases MEF2 Transcriptional Activity, Metabolic Gene Expression, and Oxidative Metabolism In Vitro

We sought to identify an HDAC inhibitor that could induce similar phenotypic adaptations. We reasoned that these effects could be obtained through three different mechanisms: (1) inhibition of HDAC3, which is part of the class IIa HDAC corepressor complex; (2) direct inhibition of the class IIa HDACs; and/or (3) class IIa HDAC corepressor complex disruption. Three compounds—TSA (trichostatin A), Scriptaid, and MC1568—with different physicochemical properties were examined. TSA has high selectivity against class I HDACs (Bradner et al., 2010), while MC1568 is reportedly a class IIa-specific inhibitor (Mai et al., 2005). In contrast, Scriptaid shows weak inhibitory activity against class I HDACs (Bradner et al., 2010) but has a large capping region, the size of which has been linked to the capacity to disrupt the class IIa HDAC corepressor complex (Hudson et al., 2015). When administered to C2C12 myotubes, TSA and Scriptaid at 0.1 and 1 μ M increased histone 3 lysine 9 acetylation (H3K9ac; Figure 2A). As some HDAC inhibitors have reported context-dependent cytotoxicity (Zhang et al., 2013), lactate dehydrogenase (LDH) release from myotubes in response to a therapeutically relevant dose (1 μ M) of TSA, Scriptaid, and MC1568 was assessed. TSA increased LDH release, indicating reduced cell viability (Figure 2B), and was excluded from further analyses. Time-dependent expression profiling of candidate exercise-responsive metabolic genes in myotubes treated with Scriptaid or MC1568 for 60 min revealed that Scriptaid increased the expression of genes involved in lipid metabolism, mitochondrial biogenesis, and mitochondrial function (Figure 2C). Unexpectedly, MC1568 reduced the expression of all genes examined (Figure 2C). In addition to our recent structural reassignment of this compound (Fleming et al., 2014), we also found that MC1568 did not elicit inhibitory activity toward HDAC4 and HDAC5 against the class IIa HDAC-specific trifluoroacetyl-lysine substrate in cell-free assays (Figure S2A). Therefore, MC1568 was excluded from further analyses. Scriptaid increased MEF2-dependent transcriptional activity (Figure 2D) and basal OCR (Figure 2E). This was due to accelerated ATP turnover, and maximal respiratory capacity was also increased (Figure 2F). Scriptaid also increased palmitate oxidation (Figure 2G). These data show that Scriptaid enhanced metabolic gene expression, energy expenditure, and lipid oxidation and was selected for further mechanism of action and *in vivo* efficacy studies.

Scriptaid Alters Class IIa HDAC/Corepressor Interactions

Scriptaid action on class IIa HDAC function was assessed. To our knowledge, no studies have examined the inhibitory activity of Scriptaid against the class IIa HDACs for the non-physiological synthetic trifluoroacetyl-lysine substrate. In cell-free assays

with recombinant HDAC isoforms, Scriptaid had only very weak inhibitory activity against HDAC3 (IC_{50} [half maximal inhibitory concentration], 0.5 μ M; Figure S3), HDAC4, and HDAC5 (IC_{50} 20 μ M and 0.5 μ M, respectively; Figure S2B). In addition to the fact that no physiological trifluoroacetyl-lysine substrates have been identified, this suggests that the action of Scriptaid on metabolic adaptation in muscle cells occurs independently of direct inhibition of class I and IIa HDACs. Some HDAC inhibitors can impair class IIa HDAC corepressor associations, which appear dependent on the compound's capping group (Hudson et al., 2015). As Scriptaid possesses a larger capping region than most hydroxamate-zinc-chelating HDAC inhibitors, we hypothesized that Scriptaid impairs class IIa HDAC corepressor interactions. Indeed, in high-throughput proteomics analyses, Scriptaid has been observed to dissociate a number of coregulator complex proteins from HDAC enzymes (Bantscheff et al., 2011). Docking of Scriptaid to HDAC4 revealed a binding pose consistent with that of HDAC inhibitors (Figure 3A). The hydroxamic acid exhibits a bidentate interaction with the active-site zinc, while the aliphatic chain occupies the cleft. The large tricyclic capping region is exposed outside of the active site in close proximity to F812 and F871, which comprise the binding tunnel. This optimal binding orientation is consistent with reports that Scriptaid has a higher binding affinity (~4- to 5-fold) with the class IIa HDACs, compared with other HDAC classes (Bantscheff et al., 2011). To determine whether Scriptaid disrupts the class IIa corepressor complex, HDAC4 interaction with the corepressor SMRT was assessed by anisotropy assays using a fluorescence-labeled peptide corresponding to amino acids 1,450–1,469 of SMRT, which contains a class IIa HDAC-interacting domain (Hudson et al., 2015). Scriptaid reduced the maximal interaction polarization between wild-type (WT) HDAC4 and the SMRT peptide (Figure 3B), suggesting that Scriptaid binding influences the mobility of the fluorophore on the SMRT peptide, implying proximity of binding. Furthermore, Scriptaid reduced the binding affinity (higher dissociation constant, K_D) between the SMRT peptide and a gain-of-function (GOF) HDAC4 mutant (H976Y) that enhances its association with SMRT (Figure 3B). This was further analyzed *in vivo*, where Scriptaid was acutely administered to mice via intraperitoneal (i.p.) injection. A time and dose-response analysis of tissue H3K9ac was used to estimate Scriptaid pharmacokinetics. Scriptaid at 1 mg/kg was sufficient to increase H3K9ac in the EDL (Figure 3C), with less obvious alterations in H3K9ac in the pancreas and brain (Figure S3A). Modest increases in H3K9ac were also observed in the heart, while H3K9ac appeared to be reduced in the liver (Figure S3A). Scriptaid at 3 and 10 mg/kg body weight did not appear to have additional effects on H3K9ac in skeletal muscle (data not shown). Therefore, Scriptaid at 1 mg/kg body weight, which is an acceptable effective therapeutic dose, was used for all future experiments. Scriptaid reduced MEF2-associated SMRT in EDL muscle 60 min after its administration (Figure 3D), while MEF2 DNA binding capacity was increased (Figure 3E). Scriptaid had no effect on the phosphorylation of the class IIa HDACs (Figure S3B), which regulates class IIa HDAC corepressor interactions and the nuclear export of class IIa HDACs. Together, these data suggest that Scriptaid disrupts the class IIa HDAC corepressor complex.

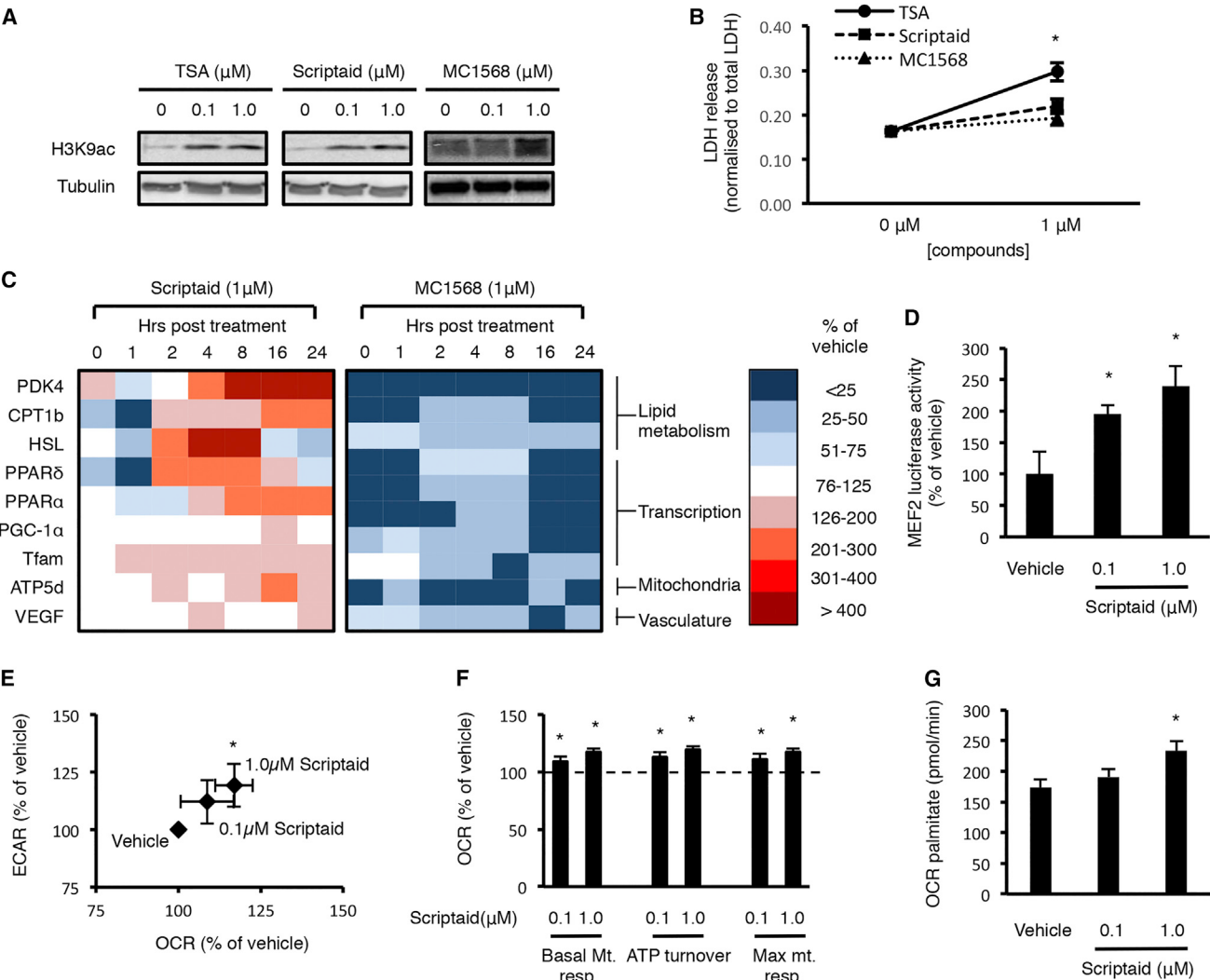


Figure 2. Pharmacological HDAC Inhibition Increases MEF2 Transcriptional Activity, Metabolic Gene Expression, and Oxidative Metabolism In Vitro

(A) C2C12 myotube histone 3 lysine 9 acetylation (H3K9ac) following 60-min exposure to vehicle (DMSO) or 0.1 μM or 1.0 μM TSA, Scriptaid, or MC1568.
(B) Lactate dehydrogenase (LDH) release from C2C12 myotubes treated with 1 μM TSA, Scriptaid, or MC1568 for 16 hr (n = 4 biological replicates per group).
(C) Time course of metabolic gene expression following 60-min exposure to 1.0 μM Scriptaid or MC1568 in C2C12 myotubes. Data normalized to vehicle-treated cells (n = 4 biological replicates per time point).
(D) MEF2 luciferase reporter assays following 60-min exposure to 0.1 and 1 μM Scriptaid (n = 3 biological replicates per group).
(E–G) Basal extracellular acidification rate (ECAR) and oxygen consumption rate (OCR) (E); mitochondrial function indices (F); and palmitate oxidation in L6 myotubes treated for 2 consecutive days, 2 \times 1 hr a day, with 0.1 μM or 1.0 μM Scriptaid (G). Data were normalized to vehicle (n = 8 biological replicates per group). Mt. resp., mitochondrial respiration.
Data are mean \pm SEM. *Versus vehicle group.

Scriptaid Administration Induces Metabolic Adaptive Responses In Vivo

To examine the transcriptional response to Scriptaid and its requirement for an intact class IIa HDAC corepressor complex, one EDL muscle of C57BL6 mice was administered with rAAV6 vectors expressing DN HDAC4 and 5, while the contralateral EDL muscle was administered with empty rAAV6 vector (control) via intramuscular injection. Two weeks later, mice were administered vehicle (5% DMSO in 1 \times PBS) or Scriptaid, and skeletal

muscles were collected 4 hr later. In control EDL muscles, Scriptaid increased the expression of \sim 70% of genes with a putative MEF2 binding sequence in their promoter region (Figure 4A) and altered the expression of 1410 genes involved in a variety of biological processes, including metabolism (Figure S3C). GSEA of metabolic pathways showed that, similar to DN HDAC4 and 5, Scriptaid significantly increased fatty acid metabolism and oxidative phosphorylation pathways (Figure 4B). Indeed, these two interventions showed remarkably similar metabolic pathway

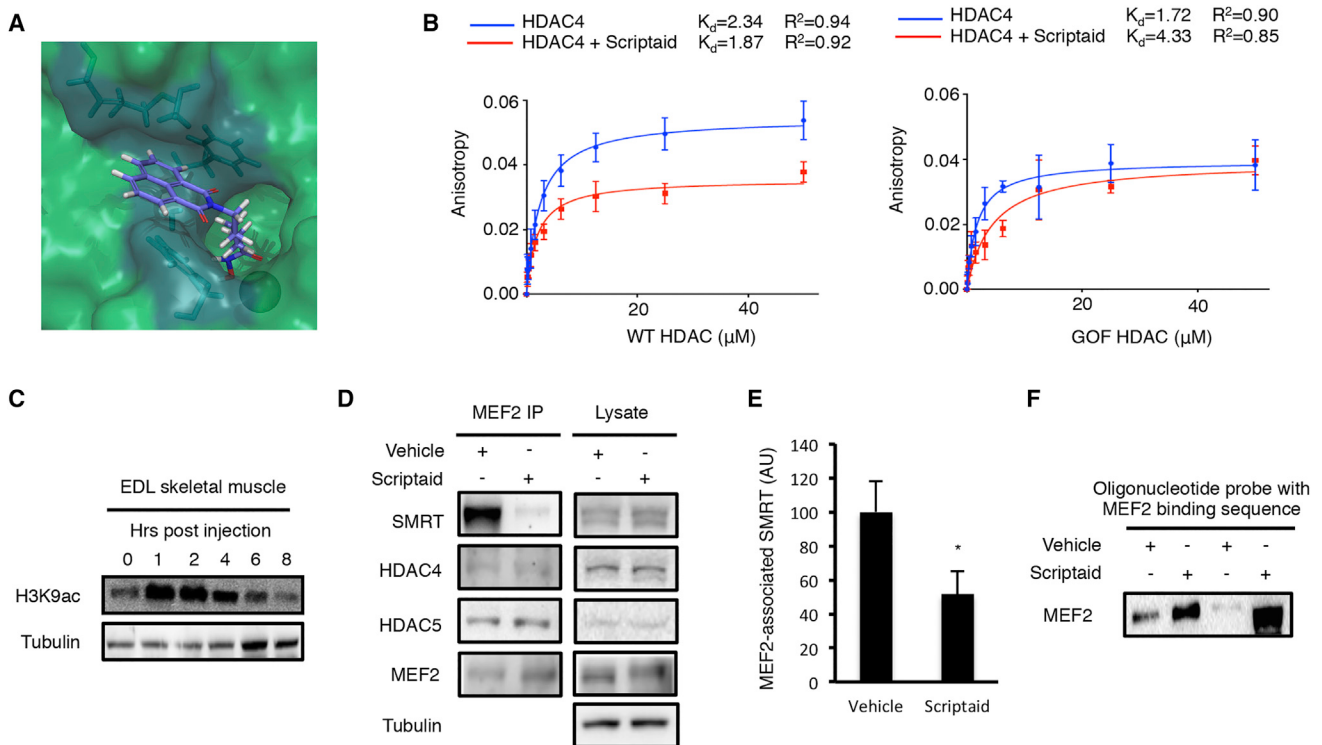


Figure 3. Scriptaid Disrupts the Class IIa HDAC Corepressor Complex

(A) Simulation of Scriptaid docking with the active site of HDAC4. Scriptaid coordinates with the active-site zinc (sphere) and its capping region interacts with F residues (teal) around the rim of the catalytic groove.

(B) Fluorescence anisotropy of WT and gain-of-function (GOF) mutant (H976Y) HDAC4 and a peptide corresponding to amino acids 1,450–1,469 of SMRT in the absence or presence of 2 M excess Scriptaid. Dissociation constants are given in micromolar.

(C) Histone 3 lysine 9 acetylation (H3K9ac) in the EDL muscle at 0, 1, 2, 4, 6, and 8 hr after a single administration of 1 mg/kg body weight of Scriptaid via intraperitoneal (i.p.) injection.

(D–F) Coimmunoprecipitation of the class IIa HDAC corepressor complex (D); MEF2-associated SMRT ($n = 8$ per group) (E); and MEF2 DNA binding in EDL muscles of mice administered vehicle (5% DMSO in 1× PBS) or 1 mg/kg Scriptaid (F).

Data are mean \pm SEM. *Versus vehicle group.

gene expression alterations (Figure S3D), suggesting that Scriptaid exerts many of its effects on skeletal muscle transcription through HDAC4 and 5. This was assessed directly by comparing the effects of Scriptaid on the expression of a selection of metabolic genes in control and EDL muscles expressing DN HDAC4 and 5. Scriptaid tended to increase all genes examined in control muscles and significantly increased *SDHb*, *ATP5d*, *CPT-1b*, and *PPARδ* (Figure 4C). In contrast, Scriptaid either did not alter or decreased these same genes in muscles in which DN HDAC4 and 5 were expressed (Figure 4C). Together, these data provide evidence that Scriptaid regulates a network of metabolic genes in vivo, which is dependent on normal class IIa HDAC function.

To assess whether chronic Scriptaid administration enhances functional capacity and metabolism in vivo, mice were treated with 1 mg/kg Scriptaid via daily i.p. injection for 4 weeks. Scriptaid treatment did not alter body weight (Figure S4A) or composition (Figures S4B and S4C) but did increase food intake (Figure S4D). Consistent with Scriptaid-mimicking aspects of the exercise-adaptive response, Scriptaid-treated mice had a greater time to fatigue than vehicle-treated mice in a treadmill-based incremental exercise test (Figure 4D). Consistent with

in vitro observations, Scriptaid invoked a small but significant increase in whole-body energy expenditure (Figure 4E) and lipid oxidation (Figure 4F). There was no effect on carbohydrate oxidation (Figure 4G) or voluntary activity (Figure S4E). Respiration analyses were performed to determine the tissues contributing to these effects. Scriptaid administration increased ADP-stimulated respiration in EDL muscle (Figure 4H), which was associated with greater respiration linked to ATP production, but not uncoupled respiration (Figure 4I). Scriptaid administration had no effect on respiration in liver (Figure S4F) or white adipose tissue (Figure S4G), although a role for brown fat could not be excluded, which tended to be higher in Scriptaid-treated animals, but was not significantly different (Figure S4H). Together with enhanced exercise capacity, these data suggest that skeletal muscle is the major tissue for Scriptaid action. Scriptaid had limited effects on skeletal muscle expression of metabolic genes when assessed 24 hr after the last administration (Figure S4I), but it did increase PGC-1 α , HSL (Figure S4J), and mitochondrial complex protein abundance (Figure 4J). Scriptaid reduced a number of plasma lipids, including specific species of dihydroceramides, ceramides, sphingomyelins, and

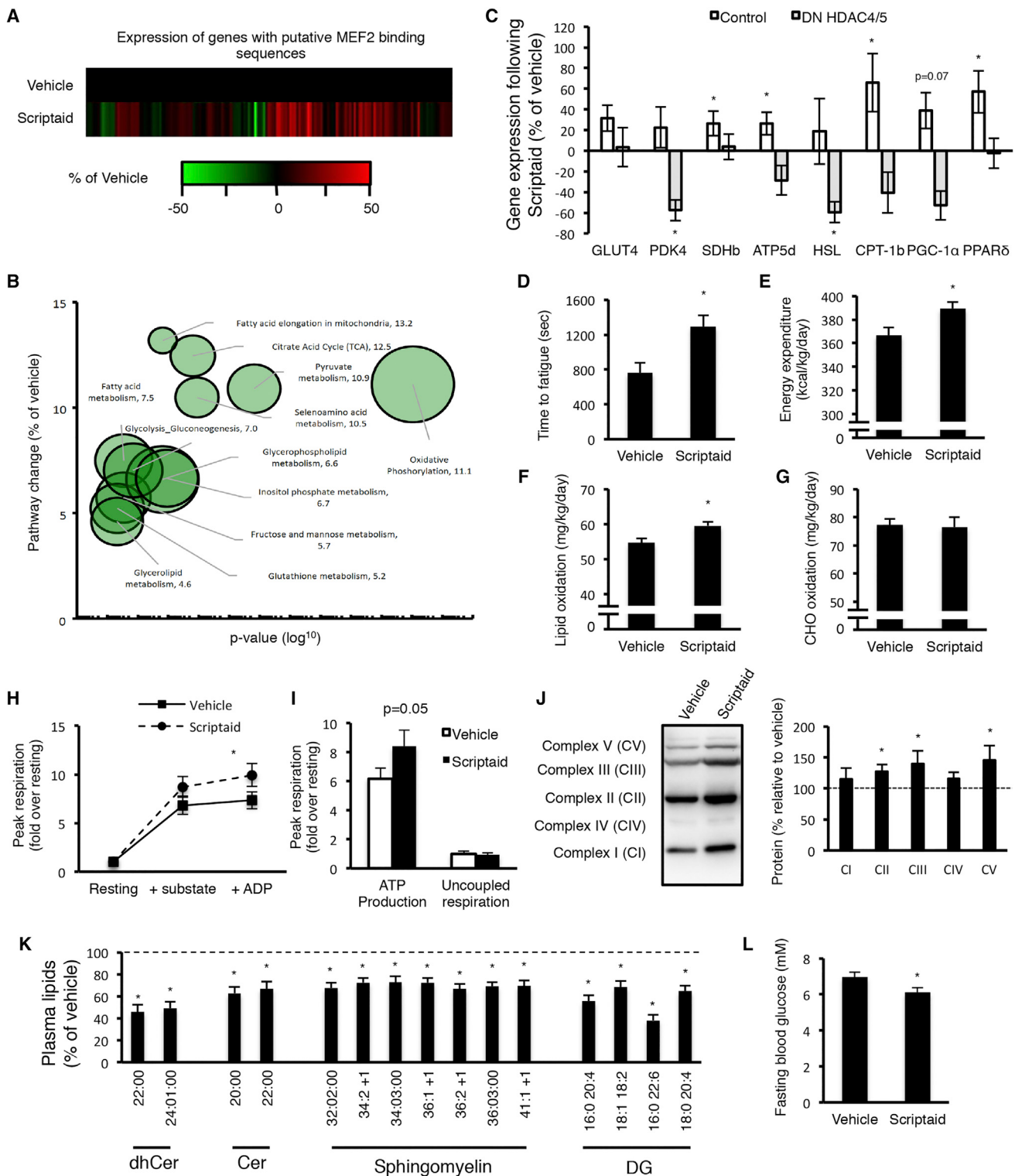


Figure 4. The Effects of Scriptaid In Vivo

(A–C) Expression of genes with putative MEF2 promoter sequences (A); bubble-plot representation of GSEA of significantly altered metabolic pathways (B); and expression of metabolic genes 4 hr after 1 mg/kg body weight Scriptaid administration in EDL muscles administered empty rAAV6 (Control) or rAAV6 DN HDAC4 and rAAV6 DN HDAC5 (n = 6 per group) (C).

(legend continued on next page)

diacylglycerides (Figure 4K), in addition to total ceramides and total dihydroceramides (Figures S4N and S4O). Scriptaid also reduced fasting blood glucose levels (Figure 4L) in the absence of changes in circulating insulin (Figure S4P). Importantly, there were no adverse effects on cardiac morphology in Scriptaid-treated mice (Figure S4Q). These data show that chronic Scriptaid administration induces metabolic adaptations in vivo, including enhanced whole-body energy expenditure and lipid oxidation and reduced plasma lipids and glucose.

DISCUSSION

This study has used previous observations on the molecular responses to exercise to validate the class IIa HDACs as effective targets to pharmacologically manipulate aspects of the exercise adaptive response. Disruption of the class IIa HDAC corepressor complex through genetic or pharmacological strategies increased the expression of exercise-responsive genes in skeletal muscle, enhanced exercise performance, increased whole-body energy expenditure and fatty acid oxidation, and reduced blood lipids and glucose. Although an increase in energy expenditure was observed in mice treated with Scriptaid, no alterations in body composition were observed, due to a small increase in food intake. Nonetheless, Scriptaid treatment reduced the levels of a number of plasma lipids that have been linked to obesity and type 2 diabetes (Meikle et al., 2013), cardiovascular diseases (Fernandez et al., 2013), and non-alcoholic fatty liver disease (Gorden et al., 2015). The broad-spectrum inhibitory profile of this compound toward a number of HDAC isoforms would likely preclude its use in chronic disease states. Nonetheless, these studies provide the impetus for the development of compounds to specifically target the class IIa HDACs and/or its corepressor complex in metabolic diseases.

In conclusion, this study has validated the class IIa HDACs as targets to pharmacologically enhance skeletal muscle metabolic adaptations, including enhanced functional capacity, energy expenditure, and lipid oxidation. This approach could be a useful prevention strategy to enhance metabolic health in chronic diseases.

EXPERIMENTAL PROCEDURES

Mouse HDAC4 and HDAC5 cDNA were sub-cloned into an AAV expression plasmid. AAV6 pseudotyped vectors containing the muscle-specific CK6 promoter (Gregorevic et al., 2004) were packaged, purified, and titrated as previously described (Winbanks et al., 2013). MC1568 was synthesized using previously described procedures (Fleming et al., 2014). Scriptaid and TSA were purchased from Santa Cruz Biotechnology and Sigma-Aldrich, respectively. All animal experiments were approved by the Deakin University Animal Welfare Committee, which is subject to the Australian Code for the Responsible Conduct of Research. Male, 8-week-old C57BL6 mice were obtained from the Animal Resource Centre in Western Australia. For AAV experiments, mice were anesthetized with isoflurane before intramuscular injection of rAAV6 vectors expressing D832N HDAC4 and D861N HDAC5 into the anterior

and posterior compartments of the hindlimb targeting the soleus, TA, and EDL muscles. Each 30- μ l injection contained 2.5×10^{10} vector genomes of each mutant HDAC vector diluted in Hank's balanced salt solution (HBSS). Control injections of the contralateral limb included 5.0×10^{10} vector genomes of empty rAAV6 vector in 30 μ l of HBSS. Scriptaid and vehicle (5% DMSO in 1× PBS) were administered via i.p. injection. For chronic drug administration studies, mice received single daily i.p. injections of Scriptaid (1 mg/kg body weight) or vehicle (5% DMSO in 1× PBS) in the afternoon ($n = 10$ per group) for 28 days until they were humanely killed. In the final 14 days of treatment, 24 hr of indirect calorimetry, an incremental exercise test, and body composition analysis by EchoMRI were performed. Mice were fasted overnight prior to cervical dislocation and tissue collection. Bioenergetic and mitochondrial function assays were performed as previously described (Martin et al., 2014; Selathurai et al., 2015). Detailed materials and methods for all other procedures can be found in the *Supplemental Information*. All data are expressed as means \pm SEM. Data normality was assessed using SPSS statistical software. For normally distributed data, differences between groups were assessed with a t test or one-way ANOVA as appropriate, using Minitab statistical software. Specific differences between groups were identified using Tukey post hoc tests. For non-normally distributed data, we performed non-parametric tests using SPSS statistical software. Differences were considered statistically significant where $p < 0.05$.

ACCESSION NUMBERS

The accession number for the microarray dataset reported in this paper is GEO: GSE54642.

SUPPLEMENTAL INFORMATION

Supplemental Information includes Supplemental Experimental Procedures and four figures and can be found with this article online at <http://dx.doi.org/10.1016/j.celrep.2016.08.005>.

AUTHOR CONTRIBUTIONS

M.H. and S.L.M. conceived the research. V.G., T.C., K.R.W., M.H., and S.L.M. designed experiments. V.G., T.C., A.S., C.R.B., D.C.H., S.D.M., S.T.B., K.A.M., L.K.-B., T.D.A., M.W., L.S.P.W., D.C., and G.M.H. performed experiments and analyzed data. C.F., J.W.R.S., K.B., M.A.F., P.G., and F.M.P. provided technical expertise and reagents. V.G., T.C., and S.L.M. wrote the manuscript. All authors edited and approved the manuscript.

ACKNOWLEDGMENTS

The authors wish to thank Assoc. Prof. Peter Meikle (Metabolomics Laboratory, Baker IDI) for assistance with lipid analysis, Hongwei Qian for AAV production, and Alex Nelson for technical assistance. This research was supported by the Diabetes Australia Research Trust Viertel Award and by grants from the National Health and Medical Research Council (NHMRC) of Australia (1027727) and the Deakin University Molecular and Medical Research Strategic Research Centre to S.L.M. J.W.R.S. is supported by Wellcome Trust Senior Investigator Award WT100237 and is a Royal Society Merit Award Holder. M.A.F., P.G., and S.L.M. are supported by research fellowships from the NHMRC.

Received: September 2, 2015

Revised: June 20, 2016

Accepted: July 31, 2016

Published: September 13, 2016

(D–L) Incremental treadmill test time to fatigue (D); whole-body energy expenditure (E); lipid oxidation (F); carbohydrate (CHO) oxidation (G); substrate (malate, succinate glutamate) and ADP-stimulated respiration in EDL muscle (H); ATP-linked and uncoupled respiration in EDL muscle (I); oxidative phosphorylation complex subunit protein in EDL muscle (J); fasting (16 hr) plasma lipids (K); and fasting (16 hr) blood glucose in mice treated with 1 mg/kg body weight Scriptaid or vehicle (5% DMSO in 1× PBS) via daily i.p. injection ($n = 9$ –10 per group) (L). Data are means \pm SEM. *Versus vehicle-treated group.

REFERENCES

- Bantscheff, M., Hopf, C., Savitski, M.M., Dittmann, A., Grandi, P., Michon, A.M., Schlegl, J., Abraham, Y., Becher, I., Bergamini, G., et al. (2011). Chemoproteomics profiling of HDAC inhibitors reveals selective targeting of HDAC complexes. *Nat. Biotechnol.* 29, 255–265.
- Booth, F.W., Roberts, C.K., and Laye, M.J. (2012). Lack of exercise is a major cause of chronic diseases. *Compr. Physiol.* 2, 1143–1211.
- Bradner, J.E., West, N., Grachan, M.L., Greenberg, E.F., Haggarty, S.J., Warnow, T., and Mazitschek, R. (2010). Chemical phylogenetics of histone deacetylases. *Nat. Chem. Biol.* 6, 238–243.
- Egan, B., and Zierath, J.R. (2013). Exercise metabolism and the molecular regulation of skeletal muscle adaptation. *Cell Metab.* 17, 162–184.
- Fernandez, C., Sandin, M., Sampaio, J.L., Almgren, P., Narkiewicz, K., Hoffmann, M., Hedner, T., Wahlstrand, B., Simons, K., Shevchenko, A., et al. (2013). Plasma lipid composition and risk of developing cardiovascular disease. *PLoS ONE* 8, e71846.
- Fischle, W., Dequiedt, F., Hendzel, M.J., Guenther, M.G., Lazar, M.A., Voelter, W., and Verdin, E. (2002). Enzymatic activity associated with class II HDACs is dependent on a multiprotein complex containing HDAC3 and SMRT/N-CoR. *Mol. Cell* 9, 45–57.
- Fleming, C.L., Ashton, T.D., Gaur, V., McGee, S.L., and Pfeffer, F.M. (2014). Improved synthesis and structural reassignment of MC1568: a class IIA selective HDAC inhibitor. *J. Med. Chem.* 57, 1132–1135.
- Gorden, D.L., Myers, D.S., Ivanova, P.T., Fahy, E., Maurya, M.R., Gupta, S., Min, J., Spann, N.J., McDonald, J.G., Kelly, S.L., et al. (2015). Biomarkers of NAFLD progression: a lipidomics approach to an epidemic. *J. Lipid Res.* 56, 722–736.
- Gregorevic, P., Blankinship, M.J., Allen, J.M., Crawford, R.W., Meuse, L., Miller, D.G., Russell, D.W., and Chamberlain, J.S. (2004). Systemic delivery of genes to striated muscles using adeno-associated viral vectors. *Nat. Med.* 10, 828–834.
- Hudson, G.M., Watson, P.J., Fairall, L., Jamieson, A.G., and Schwabe, J.W. (2015). Insights into the recruitment of class IIA histone deacetylases (HDACs) to the SMRT/NCoR transcriptional repression complex. *J. Biol. Chem.* 290, 18237–18244.
- Kao, H.Y., Downes, M., Ordentlich, P., and Evans, R.M. (2000). Isolation of a novel histone deacetylase reveals that class I and class II deacetylases promote SMRT-mediated repression. *Genes Dev.* 14, 55–66.
- Lahm, A., Paolini, C., Pallaoro, M., Nardi, M.C., Jones, P., Nedermann, P., Sambucini, S., Bottomley, M.J., Lo Surdo, P., Carfi, A., et al. (2007). Unraveling the hidden catalytic activity of vertebrate class IIA histone deacetylases. *Proc. Natl. Acad. Sci. USA* 104, 17335–17340.
- Mai, A., Massa, S., Pezzi, R., Valente, S., Loidl, P., and Brosch, G. (2005). Synthesis and biological evaluation of 2-, 3-, and 4-acylaminoctannyl-N-hydroxyamides as novel synthetic HDAC inhibitors. *Med. Chem.* 1, 245–254.
- Martin, S.D., Morrison, S., Konstantopoulos, N., and McGee, S.L. (2014). Mitochondrial dysfunction has divergent, cell type-dependent effects on insulin action. *Mol. Metab.* 3, 408–418.
- McGee, S.L., and Hargreaves, M. (2004). Exercise and myocyte enhancer factor 2 regulation in human skeletal muscle. *Diabetes* 53, 1208–1214.
- McGee, S.L., Sparling, D., Olson, A.L., and Hargreaves, M. (2006). Exercise increases MEF2- and GEF DNA-binding activity in human skeletal muscle. *FASEB J.* 20, 348–349.
- McGee, S.L., Fairlie, E., Garnham, A.P., and Hargreaves, M. (2009). Exercise-induced histone modifications in human skeletal muscle. *J. Physiol.* 587, 5951–5958.
- McKinsey, T.A., Zhang, C.L., and Olson, E.N. (2001). Control of muscle development by dueling HATs and HDACs. *Curr. Opin. Genet. Dev.* 11, 497–504.
- Meikle, P.J., Wong, G., Barlow, C.K., Weir, J.M., Greeve, M.A., MacIntosh, G.L., Almasy, L., Comuzzie, A.G., Mahaney, M.C., Kowalczyk, A., et al. (2013). Plasma lipid profiling shows similar associations with prediabetes and type 2 diabetes. *PLoS ONE* 8, e74341.
- Mokdad, A.H., Marks, J.S., Stroup, D.F., and Gerberding, J.L. (2004). Actual causes of death in the United States, 2000. *JAMA* 291, 1238–1245.
- Selathurai, A., Kowalski, G.M., Burch, M.L., Sepulveda, P., Risis, S., Lee-Young, R.S., Lamont, S., Meikle, P.J., Genders, A.J., McGee, S.L., et al. (2015). The CDP-ethanolamine pathway regulates skeletal muscle diacylglycerol content and mitochondrial biogenesis without altering insulin sensitivity. *Cell Metab.* 21, 718–730.
- Sternson, S.M., Wong, J.C., Grozinger, C.M., and Schreiber, S.L. (2001). Synthesis of 7200 small molecules based on a substructural analysis of the histone deacetylase inhibitors trichostatin and trapoxin. *Org. Lett.* 3, 4239–4242.
- Winbanks, C.E., Chen, J.L., Qian, H., Liu, Y., Bernardo, B.C., Beyer, C., Watt, K.I., Thomson, R.E., Connor, T., Turner, B.J., et al. (2013). The bone morphogenetic protein axis is a positive regulator of skeletal muscle mass. *J. Cell Biol.* 203, 345–357.
- Zhang, L., Lei, J., Shan, Y., Yang, H., Song, M., and Ma, Y. (2013). Recent progress in the development of histone deacetylase inhibitors as anti-cancer agents. *Mini Rev. Med. Chem.* 13, 1999–2013.

Supplemental Information

**Disruption of the Class IIa HDAC Corepressor
Complex Increases Energy Expenditure
and Lipid Oxidation**

Vidhi Gaur, Timothy Connor, Andrew Sanigorski, Sheree D. Martin, Clinton R. Bruce, Darren C. Henstridge, Simon T. Bond, Kevin A. McEwen, Lyndal Kerr-Bayles, Trent D. Ashton, Cassandra Fleming, Min Wu, Lisa S. Pike Winer, Denise Chen, Gregg M. Hudson, John W.R. Schwabe, Keith Baar, Mark A. Febbraio, Paul Gregorevic, Frederick M. Pfeffer, Ken R. Walder, Mark Hargreaves, and Sean L. McGee

SUPPLEMENTARY FIGURE 1

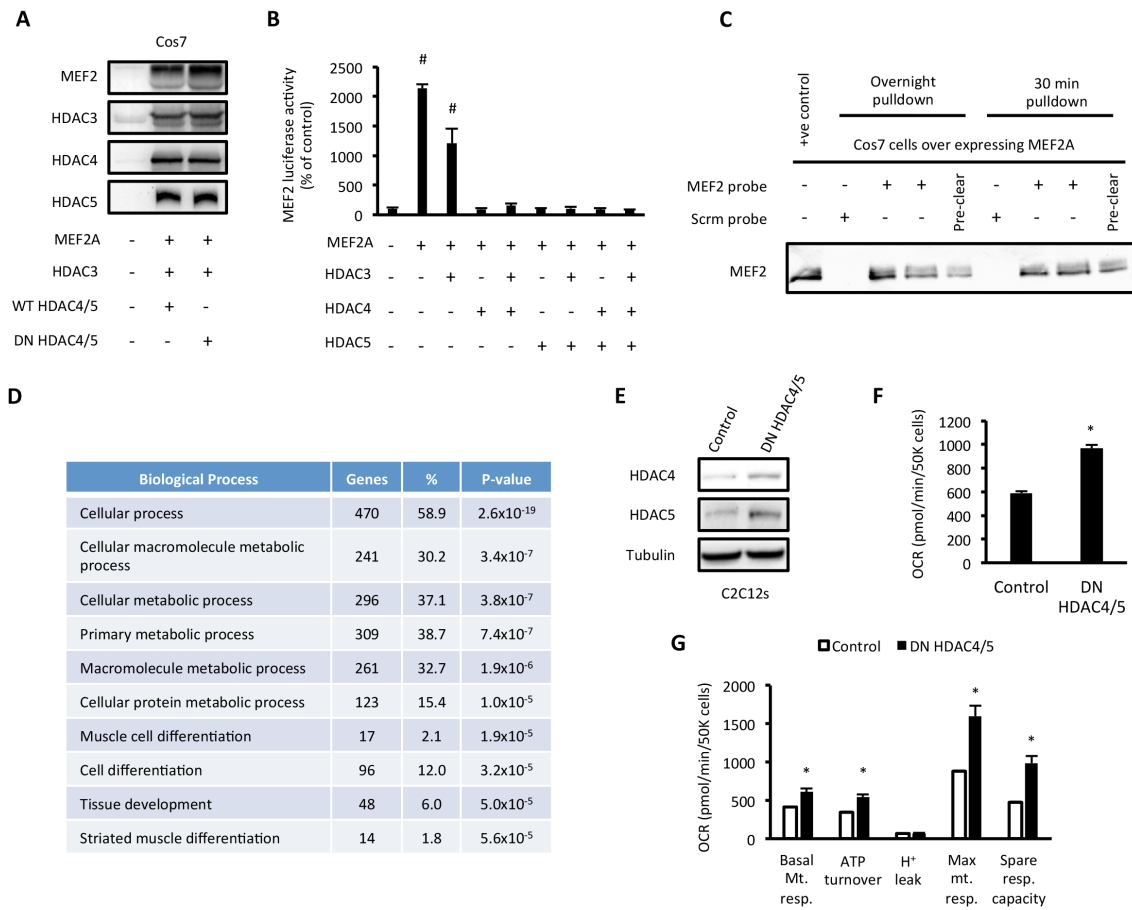


Figure S1: Active site mutant (DN) HDAC4 and 5 increase MEF2 transcriptional activity, the expression of exercise-responsive genes and oxidative metabolism. Related to Figure 1 (A) Over expression of MEF2A, HDAC3 and wild type (WT) and dominant negative (DN) HDAC4 and 5 (D832N HDAC4 and D861N HDAC5) in Cos7 cells. (B) MEF2 luciferase reporter assays with various combinations of MEF2A, HDAC3, 4 and 5. (C) Validation of MEF2 DNA binding assay using biotin labelled oligonucleotide probes and Streptavidin agarose beads in lysates of Cos7 cells overexpressing MEF2A. (D) Biological processes significantly altered following DN HDAC4 and HDAC5 over expression in EDL muscle identified by gene set enrichment analysis (n=5/group). (E) HDAC4 and 5 protein; (F) Basal oxygen consumption rate (OCR), and; (G) Mitochondrial function indices in C2C12 myotubes administered empty rAAV6 (Control) or rAAV6 DN HDAC4 and rAAV6 DN HDAC5 (n=5 biological replicates/group). Data represented as mean \pm SEM. # Denotes significantly different from all other groups *Denotes significantly different from control. ‡Denotes significant over representation within the data set.

SUPPLEMENTARY FIGURE 2

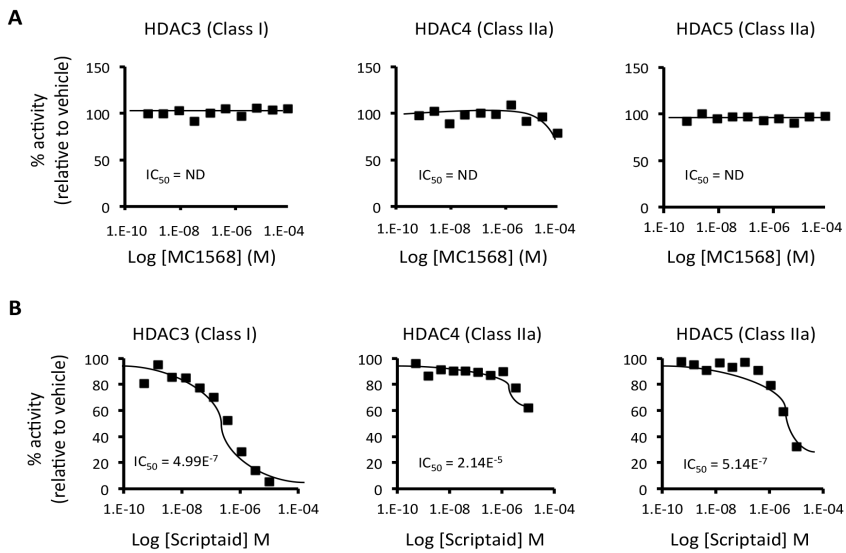


Figure S2: Inhibitor activity of compounds against various HDAC isoforms. Related to Figures 2 and 3. Cell free HDAC assays with purified HDAC3-5 and isoform specific substrates (truncated p53 peptide for class I and IIb HDACs and trifluoroacetyl lysine for class IIa HDACs), incubated in the presence of increasing concentrations of MC1568 (A) or Scriptaid (B).

SUPPLEMENTARY FIGURE 3

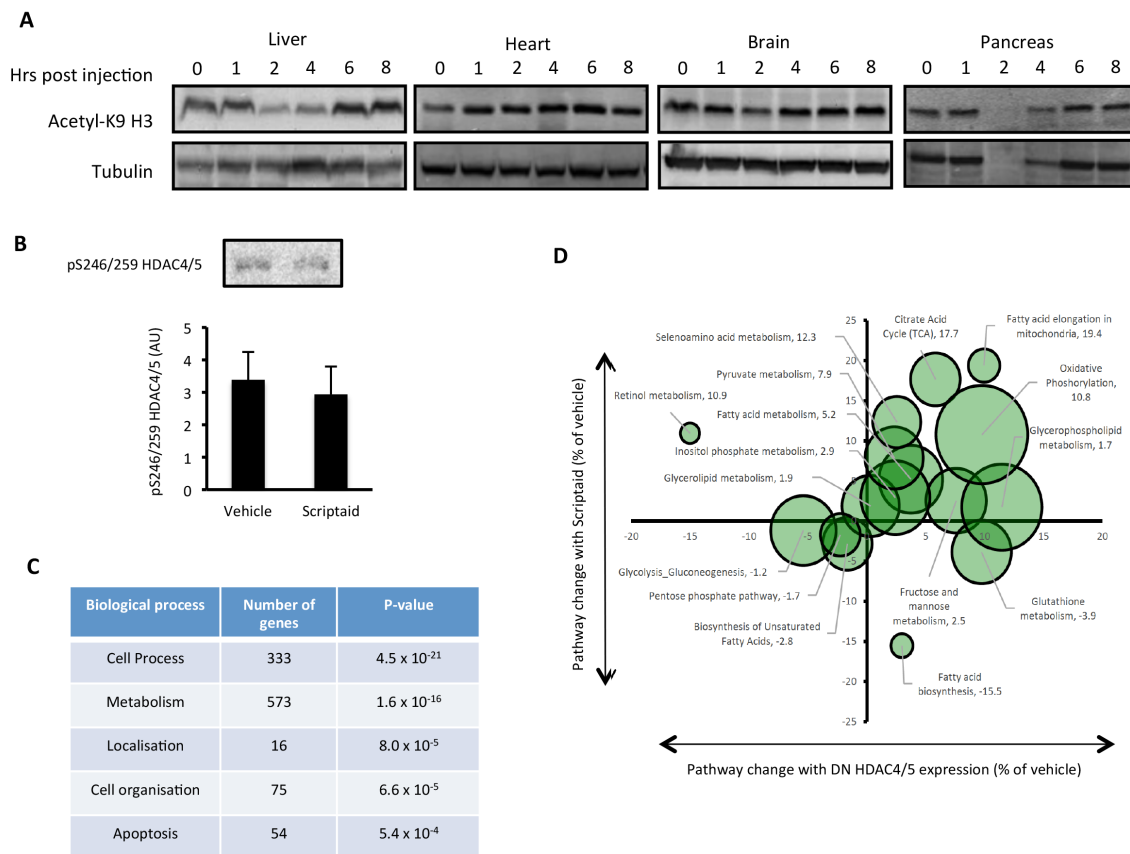


Figure S3: Acute Scriptaid administration induces metabolic adaptive responses *in vivo*. Related to Figures 3 and 4. (A) Histone 3 lysine 9 acetylation (acetyl- K9 H3) in the liver, heart, brain and pancreas at 0, 1, 2, 4, 6 and 8hr after a single administration of 1mg/kg body weight of Scriptaid via intraperitoneal (i.p) injection. (B) Phosphorylation of HDAC4 and 5 at S246 and S259, respectively, 4hr after a single administration of 1mg/kg body weight of Scriptaid in the EDL muscle. (C) Biological processes significantly altered 4hr after a single administration of 1mg/kg body weight of Scriptaid in the EDL muscle as identified by gene set enrichment analysis (n=5/group). (D) Bubble-plot comparison of gene set enrichment analyses of metabolic pathways 4 hrs after 1mg/kg body weight Scriptaid administration (y-axis) and by DN HDAC4 and 5 expression (x-axis). The size of each bubble is proportional to the number of genes in that pathway.

SUPPLEMENTARY FIGURE 4

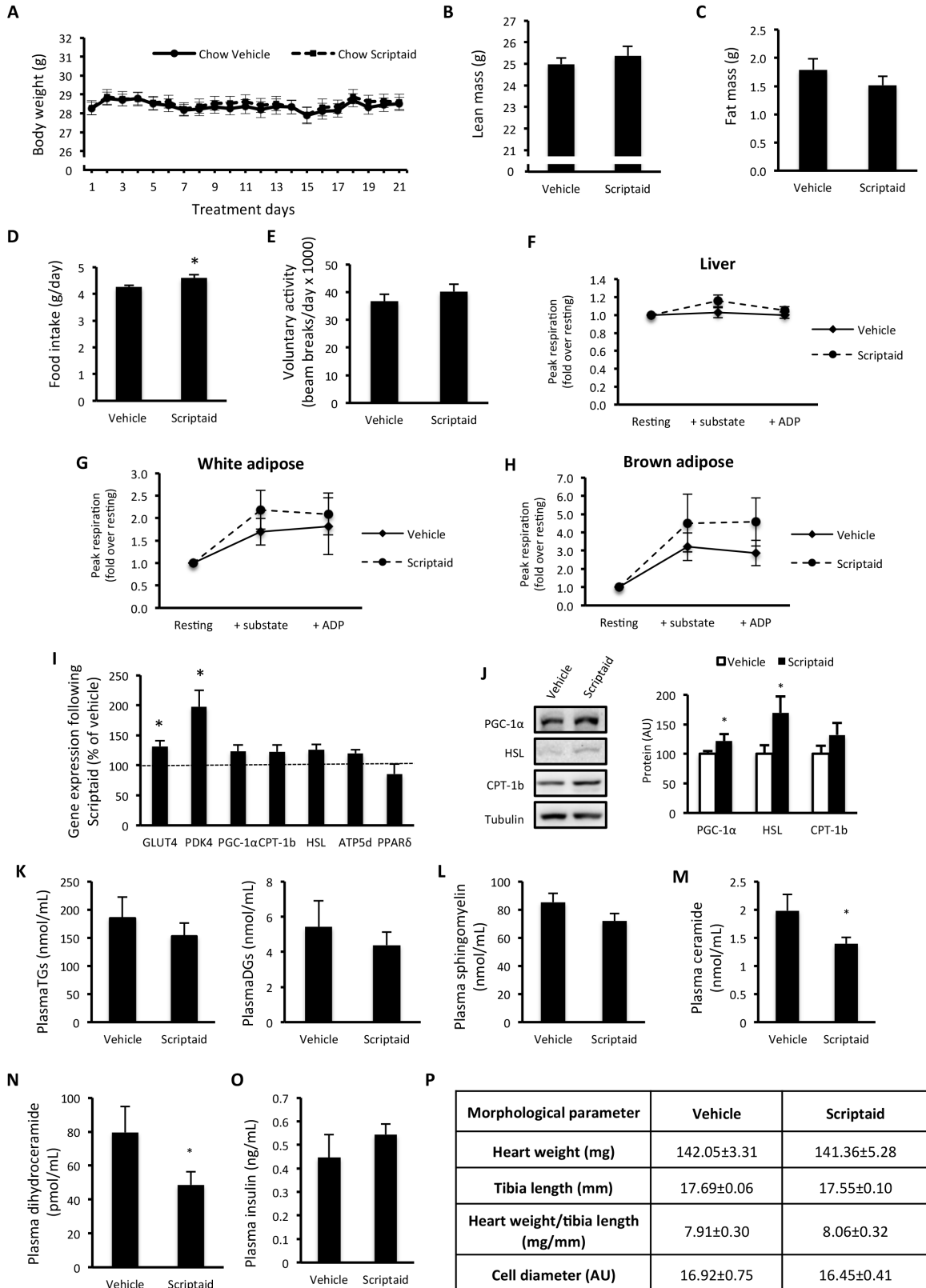


Figure S4: Chronic Scriptaid administration induces metabolic adaptive responses *in vivo*. Related to Figure 4. (A) Body weight; (B) Lean mass; (C) Fat mass; (D) Food intake; (E) Voluntary activity; Substrate (malate, succinate, glutamate) and ADP-stimulated respiration in the Liver (F), white adipose tissue (G) and brown adipose tissue (H); (I) Gene expression 24hr after the final Scriptaid administration in EDL muscle; (J) PGC-1 α , HSL and CPT-1b protein; (K) Plasma triglycerides (TGs); (L) Plasma diglycerides (DGs); (M) Plasma sphingomyelins; (N) Plasma ceramides; (O) Plasma dihydroceramides, (P) Plasma insulin; and; (Q) Heart weight, tibia length, heart weight/tibia length, cell diameter in mice treated with 1mg/kg body Scriptaid or vehicle (5% DMSO in 1xPBS) via daily i.p. injection (n=9-10/group). Data represented as mean \pm SEM. •Denotes statistically significant difference from Vehicle treated mice ($p<0.05$).

SUPPLEMENTAL EXPERIMENTAL PROCEDURES

Adeno-associated virus (AAV) production

Mouse HDAC4 and HDAC5 cDNA were sub-cloned into an AAV expression plasmid containing the muscle-specific CK6 promoter. D832N and D861N mutations in HDAC4 and HDAC5 respectively, were performed using the Quickchange II kit (Agilent Technologies). These plasmids were transfected into Hek293 cells, along with the pDGM6 packaging plasmid, using the calcium phosphate precipitate method, to generate pseudotype 6 vectors. 72hr after transfection, media and cells were harvested and homogenized through a microfluidizer (Microfluidics) before 0.22 μ M clarification (EMD Millipore). The purification of vectors was performed by affinity purification over a HiTrap heparin column (GE Healthcare) and spun overnight in an ultracentrifuge before being resuspended in sterile physiological Ringer's solution. Sequence specific quantitative PCR (Applied Biosystems) was used to determine vector titres.

MC1568 synthesis

General. All general reagents and solvents used for the synthesis of compounds were analytical grade (AR) and used as supplied. Anhydrous THF was dried using a *Pure Solv* (Innovative Technologies) solvent drying system. Oxalyl chloride was distilled under N₂ before use. All melting points are uncorrected and were determined using a Bibby Stuart Scientific SMP3 melting point apparatus model, Version 5.0. All NMR spectra were collected on a JEOL Eclipse JNM-Ex 270 MHz, 400 MHz FT-NMR or Bruker Avance 500SB spectrometer as specified. Samples were dissolved (0.5 mL) in either deuterated chloroform (CDCl₃) or deuterated dimethyl sulfoxide (DMSO-d₆). The residual solvent peaks specific to that of the deuterated solvents were used as an internal reference; DMSO-d₆: 2.50 ppm (¹H NMR) and 39.52 ppm (¹³C NMR), CDCl₃: 7.26 ppm (¹H NMR) and 77.0 ppm (¹³C NMR). High Resolution Mass Spectra (HRMS) analysis were conducted and recorded on an Aligent Technologies LC/MSD TOF Mass Spectrometer. Column chromatography was performed using Merck 230–400 silica gel. Petroleum Spirits refers to the fraction boiling between 40–60 °C. Those reactions that employed microwave irradiation were conducted using a CEM Discover S-Class Microwave reactor, operating at a frequency of 50/60 Hz and continuous irradiation power from 0 to 200 W. All reactions were conducted in a 10 mL microwave vial sealed with a Teflon® snap cap.

Ethyl 3-(1-methyl-1H-pyrrol-2-yl)-2-propenoate: To a stirring solution of triethyl phosphonacetate (565mg , 2.04mM ol) in THF (15 mL) at 0 °C, was added potassium *tert*-butoxide (265mg , 2.38mM ol). After 30min, a suspension of *N*-methyl-2-pyrrolecarboxaldehyde **9** (186mg , 1.70mM ol) in THF (5 mL) was added and the reaction stirred at 21 °C for 24 h. The reaction mixture was diluted with H₂O (50 mL) and the aqueous phase extracted with EtOAc (3 × 25 mL). The combined organic layer was washed with sat. NaHCO₃ (10 mL), brine (10 mL), dried overmg SO₄ and concentrated. Purification by flash column chromatography (30% Et₂O in Pet Spirits) afforded the title compound (225mg , 74%, *R*_f = 0.3) as a pale yellow oil; ¹H NMR (270 MHz, CDCl₃): δ 1.30 (t, *J* = 7.3 Hz, 3H, CH₂CH₃), 3.68 (s, 3H, NCH₃), 4.22 (q, *J* = 7.0 Hz, 2H, CH₂CH₃), 6.13 (m, 2H, pyrrole H-4, CH=CHO), 6.64 (dd, *J* = 4.1, 1.6 Hz, 1H, pyrrole H-3), 6.72 (t, *J* = 2.2 Hz, 1H, pyrrole H-5), 7.58 (d, *J* = 15.7 Hz, 1H, CH=CHO); ¹³C NMR (67.5 MHz, CDCl₃): δ 14.3, 33.7, 60.8, 109.7, 112.0, 112.7, 126.5, 129.4, 132.0, 167.9;hrMS (ESI, *m/z*): calculated for C₁₀H₁₃NO₂ [M+H]⁺ 180.1019; found 180.1026.

Ethyl 3-(5-formyl-1-methyl-1H-pyrrol-2-yl)-2-propenoate: In a 10 mL microwave vial, a solution of oxalyl chloride (213mg , 1.67mM ol) in DMF (1 mL) was stirred at 0 °C for 45min. A solution of ethyl 3-(1-methyl-1H-pyrrol-2-yl)-2-propenate **10** (100mg , 0.56mM ol) in DMF (0.5 mL) was added and the resulting reaction mixture was heated using microwave irradiation at 100 °C for 14min. After cooling to 21 °C, H₂O (9 mL) was added, affording a precipitate, which was isolated by vacuum filtration. The title compound was obtained (95mg , 83%) as a fine tan solid; mp 124–125 °C (lit. 102–104 °C)²⁰; ¹H NMR (270 MHz, DMSO-*d*₆): δ 1.25 (t, *J* = 7.1 Hz, 3H, CH₂CH₃), 3.93 (s, 3H, NCH₃), 4.20 (q, *J* = 7.1 Hz, 2H, CH₂CH₃), 6.63 (d, *J* = 15.7 Hz, 1H, CH=CHO), 6.97 (d, *J* = 4.4 Hz, 1H, pyrrole H-3), 7.06 (d, *J* = 4.4 Hz, 1H, pyrrole H-4), 7.61 (d, *J* = 15.7 Hz, 1H, CH=CHO), 9.58 (s, 1H, CHO); ¹H NMR (270 MHz, CDCl₃): δ 1.33 (t, *J* = 7.2 Hz, 3H, CH₂CH₃), 4.03 (s, 3H, NCH₃), 4.26 (q, *J* = 7.2 Hz, 2H, CH₂CH₃), 6.40 (d, *J* = 15.6 Hz, 1H, CH=CHO), 6.65 (d, *J* = 4.5 Hz, 1H, pyrrole H-3), 6.90 (d, *J* = 4.5 Hz, 1H, pyrrole H-4), 7.61 (d, *J* = 15.8 Hz, 1H, CH=CHO), 9.57 (s, 1H, CHO); ¹³C NMR (67.5 MHz, CDCl₃): δ 14.4, 32.6, 60.9, 111.0, 120.7, 124.2, 130.5, 134.1, 137.9, 166.5, 180.1; hrMS (ESI, *m/z*): calculated for C₁₁H₁₃NO₃ [M+H]⁺ 208.0968; found 208.0961.

3-(5-(3-Fluorophenyl)-3-oxo-1-propen-1-yl)-1-methyl-1H-pyrrol-2-yl)-2-propenoic acid: In a 35 mL microwave vial, a solution containing 3'-fluoroacetophenone (134mg , 0.97mM ol) and barium hydroxide octahydrate (1.220 g, 3.86mM ol) in MeOH (5 mL) was stirred at 21 °C for 15min. A solution of ethyl 3-(5-formyl-1-methyl-1H-pyrrol-2-yl)-2-propenate **12** (200mg , 0.97mM ol) was added and the reaction mixture was heated using microwave irradiation at 40 °C for 30min. The reaction mixture was diluted with H₂O (20 mL) and adjusted to pH 7 using 1 M HCl. The orange precipitate was isolated by vacuum filtration, washing thoroughly with H₂O to afford the desired compound (283mg , 98%) as an orange solid; mp 209–211 °C (lit. 210–212 °C)¹⁸; ¹H NMR (270 MHz, DMSO-*d*₆): δ 3.75 (s, 3H, NCH₃), 6.36 (d, *J* = 13.5 Hz, 1H, CH=CHOOH), 6.86 (d, *J* = 5.4 Hz, 1H, pyrrole H-3), 7.24 (d, *J* = 5.4 Hz, 1H, pyrrole H-4), 7.53 (m, 3H, CH=CHOOH, ArH-2,5), 7.74 (m, 2H, COCH=CH, COCH=CH), 7.89 (d, *J* = 8.1 Hz, 1H, ArH-4), 7.97 (d, *J* = 8.1 Hz, 1H, ArH-6); ¹³C NMR (125 MHz, DMSO-*d*₆): δ 30.5, 112.6, 114.1, 114.7 (d, ²J_{C-F} = 22.7 Hz), 117.3, 118.1, 119.7 (d, ²J_{C-F} = 21.6 Hz), 124.4 (d, ⁴J_{C-F} = 2.4 Hz), 130.9 (d, ³J_{C-F} = 8.1 Hz), 131.0, 131.8, 133.8, 134.4, 140.3 (d, ³J_{C-F} = 6.4 Hz), 162.4 (d, ¹J_{C-F} = 243.5 Hz), 167.8, 186.9 (d, ⁴J_{C-F} = 2.5 Hz); hrMS (ESI, *m/z*): calculated for C₁₇H₁₄FNO₃ [M+H]⁺ 300.1031; found 300.1032.

3-(5-(3-fluorophenyl)-3-oxo-1-propen-1-yl)-1-methyl-1H-pyrrol-2-yl)-N-hydroxy-2-propenamide (MC1568): To a stirring solution of 3-(5-(3-fluorophenyl)-3-oxo-1-propen-1-yl)-1-methyl-1H-pyrrol-2-yl)-2-propenoic acid **16** (220mg , 0.74mM ol) in CH₂Cl₂ (5 mL), was added *O*-(tetrahydro-2H-pyran-2-yl)hydroxylamine (103mg , 0.88mM ol), EDCI·HCl (456mg , 2.94mM ol), anhydrous HOEt (199mg , 1.47mM ol) and Et₃N (526mg , 5.20mM ol). After stirring at 21 °C for 16 h, the reaction mixture was transferred into a separatory funnel and was washed with brine (2 × 10 mL), dried overmg SO₄ and concentrated to dryness. Purification by flash column chromatography (2% MeOH in 1:1 EtOAc/Pet Spirits) afforded the THP-protected hydroxamic acid (202mg , 70%, *R*_f = 0.18) as a red oil that solidified upon standing. To a solution of this THP-protected hydroxamic acid (142mg , 0.356mM ol) in MeOH (10 mL), was added *p*-TsOH·H₂O (20mg , 0.107mM ol). After stirring at 21 °C for 1 h, an orange precipitate formed that was isolated by gravity filtration and further purified by recrystallisation (DMSO/H₂O), to afford the title compound (80mg , 70%) as an orange solid; mp 216–218 °C (lit. 212–215 °C)¹⁸; ¹H NMR (270 MHz, DMSO-*d*₆): δ 3.76 (s, 3H, NCH₃), 6.37 (d, *J* = 15.5 Hz, 1H, CH=CHONHOH), 6.72 (d, *J* = 4.0 Hz, 1H, pyrrole H-3), 7.25 (d, *J* = 4.0 Hz, 1H, pyrrole H-4), 7.53

(m, 3H, CH=CHONHOH, ArH-2,5), 7.75 (m, 2H, COCH=CH, COCH=CH), 7.90 (d, J = 10.2 Hz, 1H, ArH-4), 7.97 (d, J = 7.6 Hz, 1H, ArH-6), 9.03 (br s, 1H, NHOH), 10.72 (br s, 1H, NHOH); ^{13}C NMR (100 MHz, DMSO- d_6): δ 31.2, 111.6, 114.8, 115.3 (d, $^2J_{\text{C}-\text{F}}$ = 21.8 Hz), 117.9, 118.7, 120.2 (d, $^2J_{\text{C}-\text{F}}$ = 21.1 Hz), 124.9, 126.4, 131.5 (d, $^3J_{\text{C}-\text{F}}$ = 7.7 Hz), 132.5, 133.5, 135.7, 140.9 (d, $^3J_{\text{C}-\text{F}}$ = 6.3 Hz), 162.9 (d, $^1J_{\text{C}-\text{F}}$ = 243.9 Hz), 163.6, 187.4; hrMS (ESI, m/z): calculated for $\text{C}_{17}\text{H}_{15}\text{FN}_2\text{O}_3$ [M+H] $^+$ 315.1139; found 315.1138.

MEF2 reporter assays

Cos7 cells were transfected with plasmids expressing MEF2A, HDAC3, WT HDAC4, WT HDAC5 and D832N HDAC4 and D861N HDAC5 in 6 well plates before being transferred to black walled, clear bottom 96 well plates at 20K cells/well. Luciferase activity was measured 24 hrs later, and after 60 min of compound exposure for drug studies, through the addition of One-Glo reagent (Promega). Luminescence was measured using a Glomax multi-detection system (Promega).

Animal experiments

All experimental procedures were approved by the Deakin University Animal Welfare Committee (approval number A40-2010), which is subject to the Australian Code for the Responsible Conduct of Research. Male C57Bl6 mice (7/8 weeks old) were obtained from the Animal Resource Centre (WA) and were housed in the Metabolic Research Unit (MRU) Animal Facility, 2 mice per cage. All mice were housed in a temperature (22°C) and humidity controlled environment with a 12:12-h light/dark cycle, with food and water provided *ad libitum* for the duration of the study. Studies commenced after a 2 week acclimation period following the arrival of the mice at the Metabolic Research Unit Animal Facility. For AAV experiments, mice were anaesthetized with isoflurane before receiving intramuscular injections of rAAV6 vectors expressing D832N HDAC4 and rAAV6 vectors expressing D861N HDAC5 into the anterior and posterior compartments of the hindlimb targeting the soleus and EDL muscles. Each injection was 30 μL containing 2.5×10^{10} vector genomes of each mutant HDAC virus diluted in Hanks balanced salt solution (HBSS). Control injections of the contralateral limb included 5.0×10^{10} vector genomes of an empty rAAV6 vector, also in 30 μL of HBSS. Two weeks after administration, these mice were either killed by cervical dislocation without any further treatment, or were administered vehicle (5% DMSO in 1 x PBS) or Scriptaid (1mg/kg body weight; Santa Cruz Biotechnology) via intraperitoneal (i.p.) injection, before being killed by cervical dislocation 4hr later. Mice had free access to food and water after Scriptaid administration. In all mice, the EDL and soleus muscles were excised, weighed and snap frozen in liquid nitrogen. For Scriptaid dose response experiments, 10 week old male C57Bl6 mice were administered with an acute intraperitoneal (i.p.) injection of Scriptaid at 1, 3 or 10mg/kg body weight. Mice had free access to food and water after Scriptaid administration and were killed at 0, 1, 2, 4, 6 or 8hr post injection by cervical dislocation. The soleus and EDL skeletal muscles, liver, heart, pancreas and brain were collected and frozen in liquid nitrogen.

For chronic Scriptaid administration studies, 20 week old male C57Bl6 mice were assigned to either vehicle or Scriptaid groups, based on average body weight. Mice received single daily i.p. injections of Scriptaid (1mg/kg body weight) or vehicle (5% DMSO in 1 x PBS) in the afternoon (n=10 per group) until sacrificed. All mice were housed two per cage during the treatment period. After 21 days of

treatment 24hr indirect calorimetry, and an incremental exercise test was performed after 25 days. Body composition by EchoMRI scan was measured in the day prior to sacrifice. Indirect calorimetry was performed using the Fusion Metabolic system (AccuScan Instruments) USA that uses open circuit calorimetry. Mice in individual cages were monitored with environmental enrichment and ad-libitum access to water and their respective diets. To minimize the effect of environmental variations in the initial hours of recording, mice were monitored for >26hr and the final 24hr of data only was considered for calculations. The incremental exercise test was performed on an Accuscan treadmill (AccuScan Instruments, USA). All mice were familiarized with running on the treadmill two days before performing the incremental exercise test, which consisted of a starting speed of 8 meters per min (Mpm) at 0% incline. Speed was increased 2 Mpm every 2min. At 20Mpm, the grade was increased by 1% every 2min. Volitional fatigue was determined when mice could no longer run for a period > 5 sec despite manual encouragement. Blood glucose levels were determined using a glucometer after a 16hr fast and blood obtained from the tail was also collected for insulin analysis. Blood samples were collected in tubes containing ~10µL EDTA (16mM EDTA in 0.9% saline). After centrifugation at 4°C at 10,000 RPM for 10min, plasma was collected and stored at -80°C for insulin measurement, using a Mouse Insulin ELISA kit (ALPCO Diagnostics). Briefly, 5µL of standards, controls and samples combined with 75µL of conjugate were incubated for 2hr at RT with shaking at 700-900 rpm. This was followed by washing 6 times before incubation with 100µL of TMB substrate for 30min at RT with shaking at 700-900 rpm. 100µL of stop solution was added and absorbance was measured at 450nm. Body composition was determined by the EchoMRI™ Whole Body Composition Analyzer (Singapore). As per manufacturer's guide, scans were performed by placing mice into a probe with a cylindrical plastic insert added to limit their movement in a quantitative magnetic resonance (QMR) system that measures whole body fat mass, lean tissue mass, free water, and total body water, within 1min without the need for anesthesia or sedation. A recommended system test was done once a day prior to measurement scans with a canola oil test sample serving as a standard for the system test. Mice were fasted for 4hr before being killed. Blood was drawn by cardiac puncture and collected into tubes containing heparin followed by centrifugation at 4°C at 10,000 RPM for 10min and plasma collection. Tissues such as soleus and EDL skeletal muscles, liver (weighed), epididymal fat (weighed), brown fat, heart, and brain were collected, snap frozen in liquid nitrogen and stored at -80°C until analysis.

Protein extraction, Immunoprecipitation and Immunoblotting

Cells were washed with cold PBS and solubilised in 250µL cold protein lysis buffer (50mM Tris pH 7.5, 1mM EDTA, 1mM EGTA, 10% glycerol, 1% Triton X-100, 50mM NaF, 5mM sodium pyrophosphate, 1mM Na₃VO₄; 1mM DTT, 1X protease inhibitor cocktail (Sigma, St Louis, MD, USA); H₂O) on ice and rapidly frozen in liquid nitrogen. Later, thawed cell lysates were homogenised and centrifuged at 12000 rpm for 10min at 4°C and the supernatant was extracted. Tissues were homogenised in ~200-300µL cold protein lysis buffer using a hand held homogeniser, followed by centrifuging at 10000 rpm for 10min at 4°C to remove insoluble cellular debris. The total protein concentration in the cell/tissue lysates was determined using the BCA total protein kit (Pierce). For coimmunoprecipitation studies, 200µg of total protein was made up to 500µL in lysis buffer before incubation with 1µg of MEF2 antibody (H300 Santa Cruz) overnight at 4°C on a rotating wheel. The following morning, 50µL of pre-washed 50% protein A/G agarose bead slurry (Pierce) was added to each sample, prior to incubation for 2hr at 4°C on a rotating wheel. Immunocomplexes were

precipitated by centrifugation and washed three times in 1mL of 1xPBS. Immunocomplexes were eluted from agarose beads by incubating in 50µL of 2x loading buffer and were heated at 95°C for 5 min. The entire sample was analysed by SDS PAGE as described below. For immunoblotting, 50µg of protein were denatured in SDS reducing buffer and incubated at 37°C for 5min before being subjected to SDS-PAGE. Proteins were transferred onto polyvinylidene diflouride (PVDF) membranes, which were blocked in 1% bovine serum albumin in Tris-buffered saline and 0.05% Tween (TBST) for 1 hour at RT before being exposed to primary antibodies to HDAC4, HDAC5, HSL, PGC-1 α (Cell Signaling Technology) SMRT (Millipore), MEF2 (H300, Santa Cruz) CPT-1b, tubulin, acetyl-K9 H3 (Sigma-Aldrich) and oxidative phosphorylation complexes (MitoSciences) overnight, at 4°C. Membranes were washed in TBST and exposed to appropriate anti-species horseradish peroxidase (HRP) conjugated secondary antibodies for 1hr at RT, before final washes. For visualisation of MEF2 in MEF2 immunoprecipitation studies, a light chain HRP secondary antibody was used. Protein bands were detected using ECL Chemiluminescent Substrate Reagent Kit (Invitrogen) and visualized on a Chemidoc XRS System and Analysis Software (Bio-Rad Laboratories).

Oligonucleotide probe binding

An oligonucleotide probe-binding assay was used to visualize MEF2 DNA binding capacity. Two complementary oligonucleotide probes containing a consensus MEF2 binding sequence (CAAGCTGGGAGCTAAAAATAGCAGCCCCGGG) with 5' end conjugated biotin were annealed together in annealing buffer (10mM Tris pH 8.0, 50mM NaCl, 1mM EDTA) at 95°C for 3 min, before being allowed to cool gradually to room temp. A control probe with a scrambled sequence was annealed in the same way. To assess, MEF2 DNA binding, 200µg of total protein from samples were first pre-cleared with 50µL of 50% Strepavidin agarose bead slurry (Pierce) for 2hr at 4°C. The supernatant was collected and 1µg of MEF2 or oligonucleotide probe was incubated in the sample, overnight at 4°C on a rotating wheel. The following morning, 50µL of pre-washed 50% Strepavidin agarose bead slurry was added to each sample, prior to incubation for 2hr at 4°C on a rotating wheel. Double stranded oligonucleotide/protein complexes were eluted from agarose beads by incubating in 50µL of 2x loading buffer and were heated at 95°C for 5 min. The entire sample was analysed by SDS PAGE for MEF2 as described above.

Microarray analyses

RNA Quality and quantity was determined using the Agilent 2100 Bioanalyser (Agilent Technologies, Palo Alto, CA, USA) and RNA6000 NanoAssay Kit (Agilent, Melbourne, Australia) with only samples having a RIN (RNA Integrity Score) higher than 9 considered for microarray analyses. Fluorescently-labelled cDNA was prepared from 100ng RNA using Agilent's Low Input Quick-Amp Labelling protocol and One-Color RNA Spike-In kits. Cyanine 3-CTP-labelled cDNA was hybridised for 17h to Agilent Whole Mouse Genome (4x44k, G4122F Slide Kit) Oligo Microarray Slides using Agilent Gene Expression Hybridisation kit. Microarray fluorescent images were acquired using GenePix 4000B scanner, with data extraction performed using Feature Extraction Software (Version 9.5.1.1, Agilent). Only features where the processing signal was greater than 2-fold above the background were considered for further analyses. Each treatment group consisted of five biological replicates and genes were selected for further analysis if they were detected in at least three of the five replicates. Overall 23,678 genes fulfilled the selection criteria with most (greater than 90%) of those genes

having the full complement of five values for each treatment group. The resultant data was normalized to the 75th percentile value for each array as recommended by Agilent Technologies. Further microarray data analyses were performed with Excel (Microsoft) and Acuity 4 software (Molecular Devices).

The microarray dataset generated conforms to MIAME guidelines and is available at Gene Expression Omnibus (<http://www.ncbi.nlm.nih.gov/geo/query/acc.cgi>) series record GSE54642.

Identification of altered biological processes: t-tests were used to identify genes, from the normalised microarray data, with differential expression between groups of interest. No additional cut-offs were applied. These gene lists were imported into Panther (www.patherdb.org). Statistical over-representation tests using Panther Gene Ontology-Slim biological process classifications with Bonferroni correction for multiple testing. Pie charts for represented biological processes were also generated in Pather using the same classification system.

Gene Set Enrichment Analysis (GSEA): After metabolic processes were identified as a significantly over-represented in biological process analysis, GSEA was performed to examine metabolic pathway changes. Box-plots (IBM SPSS Statistics, Version 21.0. Armonk, NY: IBM Corp) were generated using the entire microarray dataset from KEGG genes lists that involved metabolism and then two-tailed Z-tests performed to identify pathways that were significantly different relative to the control group.

MEF2-dependent genes: To identify expression profiles of genes with putative MEF2 binding regions in their promoters, a list of MEF2 target genes was obtained from the Molecular Signature Database (<http://www.broadinstitute.org/gsea/msigdb/collections.jsp>). Cross-referencing these putative MEF2 genes with those in our dataset identified 167 genes. These genes were then used to generate gene expression heat-maps relative to the control group using Acuity (Molecular Devices).

Cellular bioenergetics and mitochondrial function assays

C2C12 myoblasts and L6 myoblasts were grown in Alpha minimum Essential Medium (αMEM) supplemented with 10% fetal bovine serum and 1% antibiotic-antimycotic at 37°C in a humidified 5% CO₂ incubator. Cellular bioenergetics and mitochondrial function analyses were performed using the Seahorse XF24 Extracellular Flux Analyser (Seahorse Bioscience). Cells were seeded at a density of 25K cells/well into 24 well Seahorse V7 plates. The day after seeding growth media was replaced with the differentiation media and myoblasts were differentiated to myotubes. For AAV experiments, C2C12 myotubes were administered 2x10⁵ vector genomes rAAV6 vectors expressing D832N HDAC4 and rAAV6 vectors expressing D861N HDAC5 each, or 2x10⁵ vector genomes of empty rAAV6 vector per well, on day 4 of differentiation. Media was changed 24hr later and bioenergetics assays were performed an additional 24hr later. For drug experiments, L6 myotubes were treated with 0.1μM or 1μM concentrations of Scriptaid or vehicle (DMSO) for 1hr twice per day, for 2 days, starting on day 4 of differentiation. This was designed to replicate the pulsative nature of repeated bouts of exercise. On day 6 of differentiation and 16hr after the last treatment, myotubes were assayed for the mitochondrial functional analyses. Prior to all assays, cells were washed twice with assay running media (unbuffered DMEM, 25mM glucose, 1mM glutamine and 1mM sodium pyruvate), before the final addition of 600μL of running media. The cell plate was placed in non-CO₂ incubator at 37 °C for 1hr before assay. The assay protocol consisted of repeated cycles of 4min mix,

2min wait and 2min measurement periods. Oxygen consumption rate (OCR) was simultaneously calculated through each measurement period by excitation of fluorophores for O₂ and this gives measurement of oxidative metabolism. Three basal rates of OCR were measured after three cycles before the sequential exposure of the ATP synthase inhibitor oligomycin, the proton ionophore carbonyl cyanide p-trifluoromethoxyphenylhydrazone (FCCP) and the complex III inhibitor antimycin A, all to a final concentration of 1mM, by the Seahorse injection system. Three mix, wait and measurement cycles separated each compound injection. Respiration due to ATP turnover was calculated by subtracting the mean respiration values obtained following oligomycin injection from basal respiration rates. Uncoupled respiration was calculated by subtracting the mean respiration rate obtained following antimycin A injection from that following oligomycin addition. Maximal respiratory capacity was determined by respiration following FCCP injection. Spare respiratory capacity was determined by subtracting basal respiration rate from maximal respiration. All calculations were performed on values obtained in each well and all treatment conditions were analysed as six to seven replicates, over at least two independent experiments and data was pooled to give average values for each treatment.

For respiration analyses from tissue biopsies, the tibialis anterior and EDL muscles, liver, epipldymal fat pad and subscapular brown fat pad were dissected and immediately immersed in aMEM media containing 5.7mM ATP at room temperature. The belly of the tissue was sampled using a 1mM punch biopsy needle and the tissue biopsy was then placed in a Seahorse Islet capture plate in aMEM media containing 5mM glucose. Capture plate screens were placed over the top of the muscle samples and the plate containing biopsy samples was then incubated in a non-CO₂ incubator for 10min at 30°C. Baseline respiration was measured using 2 cycles of 2min mix, 2min wait and 2min measure, before injection of malate, glutamate and succinate at final concentrations of 5mM, 1mM and 5mM respectively. Respiration was measured for two 2min periods, separated by a 2 min mix period, before injection of ADP (pH 7.4) at a final concentration of 5mM. Respiration was again measured for two 2min periods, separated by a 2 min mix period. Oligomycin was then injected (10µM final) followed by 8 measurement cycle before antimycin A was injected (10µM final), which was followed by another 8 measurements cycles. At the conclusion of the assay, the Islet Capture plate was retrieved, media and capture screens removed and the muscle samples were homogenised in 150µL of lysis buffer. Protein concentration was determined using the bicinchoninic acid (BCA) total protein kit (Pierce). All respiration values were normalised to total protein contained within each sample and state 3 respiration was established as the peak respiration values obtained following ADP injection. ATP-linked respiration was determined by subtracting the respiration value from the final measurement cycle after oligomycin injection, from the peak state 3 respiration value. Uncoupled respiration was determined by subtracting the respiration value from the final measurement cycle after antimycin A injection, from the respiration value from the final measurement cycle after oligomycin injection.

Lactate dehydrogenase release assays

Cells in 48-well plates were treated with 1µM TSA, Scriptaid or MC1568. After 24h the cytotoxic effects of these treatments were assessed using the CytoTox 96® Non-Radioactive Cytotoxicity Assay kit (Promega) as per manufacturer's instructions. Viability was expressed as LDH in the media normalised to total LDH from the media and cell lysate.

Gene expression analysis

Total mRNA from the cells was extracted by adding 350µL of RLT buffer followed by scraping, pipetting the cell lysate into a microcentrifuge tube. Total mRNA from the tissues was extracted by homogenizing ~20-30 milligrams of tissue in 1 ml of Trizol followed by incubation at room temperature (RT) for 5min. 200µL of chloroform was added to the homogenate, shaken for 15 seconds and incubated for 1min at RT before centrifuging at 12,000g for 10min at 4 °C for extracting the upper aqueous phase. An equal volume (350 µl for cell lysate/450µL for tissue) of 70% ethanol was added to cell/tissue samples and they were further purified with RNeasy spin columns (the RNeasy® min i Kit, Qiagen). Complementary DNA (cDNA) was synthesised using the SuperScript™ III transcription system (Invitrogen). cDNA was quantified by OliGreen assay (Quant-iT™ OliGreen® ssDNA Assay Kit; Invitrogen). All primers were designed in-house using the Beacon Primer Designer program software and synthesised by Gene Works (Adelaide, Australia). Primer sequence efficiency was tested over a wide concentration range and primer sequences are listed in the table below. Gene expression levels were quantified using the FastStart Universal SYBR Green Master (ROX; Roche Applied-Science) on the MX3005™ Multiplex Quantitative PCR (QPCR) system (Stratagene). Log-transformed CT values were normalised to cDNA concentration to determine relative gene expression levels.

Real-time PCR primer sequences:

Mouse CPT-1b	Forward Primer	5'- TCG CAG GAG AAA ACA CCA TGT -3'
	Reverse Primer	5'- AAC AGT GCT TGG CGG ATG TG -3'
Mouse ATP-5d	Forward Primer	5'- ACA CAG AAG ACG GCA CCA -3'
	Reverse Primer	5'- GCA CAG AGG AGT CGG CAT TC -3'
Mouse SDHb	Forward Primer	5'- TGG TGG AAC GGA GAC AAG -3'
	Reverse Primer	5'- CAG CGG TAG ACA GAG AAG G -3'
Mouse GLUT4	Forward Primer	5'- CCA GCC TAC GCC ACC ATA G -3'
	Reverse Primer	5'- TTC CAG CAG CAG CAG AGC -3'
Mouse PDK4	Forward Primer	5'- TGT GAT GTG GTA GCA GTA GTC -3'
	Reverse Primer	5'- ATG TGG TGA AGG TGT GAA GG -3'
Mouse PGC-1α	Forward Primer	5'- CCC TGC CAT TGT TAA GAC C -3'
	Reverse Primer	5'- TGC TGC TGT TCC TGT TTT C -3'
Mouse HKII	Forward Primer	5'- TGC CAA GCG TCT CCA TAA -3'
	Reverse Primer	5'- CGG AGG AAG CGG ACA TCA -3'
Mouse HSL	Forward Primer	5'- CGA GAC AGG CCT CAG TGT GA -3'
	Reverse Primer	5'- AAC TCT GGG TCT ATG GCG AAT C -3'
Mouse Cit. Syn.	Forward Primer	5'- CAA AGC TCC TGC CTG TGT TTG -3'
	Reverse Primer	5'- GGG TTT ACA GTG TGT CCA TCT CAA -3'
Mouse UCP3	Forward Primer	5'- TCGCCAGGGAGGAAGGAGTC -3'
	Reverse Primer	5'- ATGTCGTAGGTACCACATCTCAGC -3'

Mouse PPAR γ	Forward Primer	5'- TGT CTC ACA ATG CCA TCA GGT T -3'
	Reverse Primer	5'-GCT GGT CGA TAT CAC TGG AGA TC -3'
Mouse PPAR δ	Forward Primer	5'- CCT CGG GCT TCC ACT ACG -3'
	Reverse Primer	5'- CAC TTG TTG CGG TTC TTC -3'
Mouse NR4A2	Forward Primer	5'- CTG TCT CCC GCC TGT CAC TC -3'
	Reverse Primer	5'- AAG GTC TGC CCA TCC ACT ACG -3'
Mouse NRF1	Forward Primer	5'- CTG CTG TGG CTG ATG GAG AGG -3'
	Reverse Primer	5'- TGC TTG CGT CGT CTG GAT GG -3'
Mouse MHC 1	Forward Primer	5'- TGA GTT CCG ACG CCG AGA ATG -3'
	Reverse Primer	5'- TCC ACC ACA AAC ACC GAT GAC -3'
Mouse MHC 2	Forward Primer	5'- TCT CCT GCT GTT TCC TTA CTT GCT A -3'
	Reverse Primer	5'- GTA CTC CTC TGC TGA GGC TTC CT -3'
Mouse Myogenin	Forward Primer	5'- TCG GTC CCA ACC CAG GA -3'
	Reverse Primer	5'- GCA GAT TGT GGG CGT CTG TA -3'
Mouse VEGF	Forward Primer	5'- GGC TCT TCT CGC TCC GTA GTA G -3'
	Reverse Primer	5'- CCT CTC CTC TTC CTT CTC TTC CTC -3'
Mouse ADAMTS1	Forward Primer	5'- TCT ACT CTG GCA CGG TGA ACG -3'
	Reverse Primer	5'- CGC TGG CTG AAT GAA GAA CTC C -3'

Lipid Analyses

Lipids were extracted from ~10 μ L of plasma using 20 volumes of chloroform:methanol (2:1) in a single phase extraction process, recovering all lipids in a single phase suitable for liquid chromatography–mass spectrometry analysis. Lipid analyses were performed by liquid chromatography, electrospray ionisation–tandem mass spectrometry using an HP 1200 liquid chromatography system (Agilent Technologies, Santa Clara, CA, USA) combined with a PE Sciex API 4000 Q/TRAP mass spectrometer (Applied Biosystems/MDS SCIEX, Mulgrave, VIC, Australia) with a turbo-ionspray source (350°C) and Analyst 1.5 data system (Applied Biosystems/MDS SCIEX). Quantification of individual lipid species was performed using multiple-reaction monitoring (MRM) in positive ion mode. MRM product ions used were *m/z* 264 for ceramides, while diacylglycerols and triacylglycerols were monitored by the neutral loss of individual fatty acid species. Each ion pair was monitored for between 10 and 50 ms (using scheduled MRM mode), with a resolution of 0.7 amu at half-peak height, and averaged from continuous scans over the elution period. The proportionately higher signals resulting from diacylglycerol and triacylglycerol consisting of two or more identical fatty acids were corrected prior to normalisation against internal standards. Lipid concentrations were calculated by relating the peak area of each species to the peak area of the corresponding internal standards (100 pmol ceramide 17:0, 200 pmol diacylglycerol 17:0/17:0 and 100 pmol triacylglycerol 17:0/17:0/17:0), which were added prior to extraction.

Cell Free HDAC assays

Cell free HDAC assays were performed at 37°C with purified HDAC3-6. HDAC activity was monitored through deacetylation of an acetylated peptide corresponding to amino acids 379 to 382 of p53 (for HDAC3 and 6) or the class IIa specific trifluoroacetyl lysine substrate (for HDAC4 and 5). Reactions were incubated with increasing concentrations of TSA, MC1568 or Scriptaid and HDAC activity was monitored through fluorescence.

Anisotropy assays

Recombinant WT HDAC4 and HDAC4 H976Y catalytic domains were expressed in E.Coli and purified. A peptide corresponding to amino acids 1450-1469 of SMRT was synthesised by Biomatik. Peptides were conjugated to BODIPY-TMR at a 5:1 molar ration for 2hr at room temp and labelled peptides were concentrated using an Amicon centrifugal concentrator. Serial dilution anisotropy assays were performed in the presence of Scriptaid at an inhibitor:peptide ratio of 2:1 and fluorescence was recorded using an excitation wavelength of 531nm and emission wavelength of 595nm. Data were analysed assuming non-linear fit according to the equation $y = B_{max}X/(K_d + x)$.